ACS Partner Journal

Journal of the American Society for Mass Spectrometry

pubs.acs.org/jasms

Research Article

The Omnitrap Platform: A Versatile Segmented Linear Ion Trap for Multidimensional Multiple-Stage Tandem Mass Spectrometry

Dimitris Papanastasiou,* Diamantis Kounadis, Alexandros Lekkas, Ioannis Orfanopoulos, Andreas Mpozatzidis, Athanasios Smyrnakis, Elias Panagiotopoulos, Mariangela Kosmopoulou, Maria Reinhardt-Szyba, Kyle Fort, Alexander Makarov, and Roman A. Zubarev

Cite This: *J. Am. Soc. Mass Spectrom.* 2022, 33, 1990−2007

Read Online

ACCESS | Metrics & More | Article Recommendations | Supporting Information

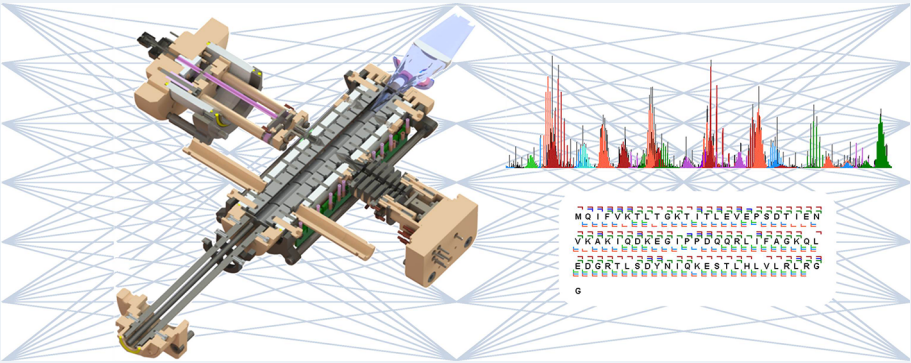

ABSTRACT: Multidimensional multiple-stage tandem processing of ions is demonstrated successfully in a novel segmented linear ion trap. The enhanced performance is enabled by incorporating the entire range of ion activation methods into a single platform in a highly dynamic fashion. The ion activation network comprises external injection of reagent ions, radical neutral species, photons, electrons, and collisions with neutrals. Axial segmentation of the two-dimensional trapping field provides access to a unique functionality landscape through a system of purpose-designed regions for processing ions with maximum flexibility. Design aspects of the segmented linear ion trap, termed the Omnitrap platform, are highlighted, and motion of ions trapped by rectangular waveforms is investigated experimentally by mapping the stability diagram, tracing secular frequencies, and exploring different isolation techniques. All fragmentation methods incorporated in the Omnitrap platform involving radical chemistry are shown to provide complete sequence coverage for partially unfolded ubiquitin. Three-stage (MS3) tandem mass spectrometry experiments combining collision-induced dissociation of radical ions produced by electron meta-ionization and further involving two intermediate steps of ion isolation and accumulation are performed with high efficiency, producing information rich spectra with signal-to-noise levels comparable to those obtained in a two-stage (MS2) experiment. The advanced capabilities of the Omnitrap platform to provide in-depth top-down MSn characterization of proteins are portrayed. Performance is further enhanced by connecting the Omnitrap platform to an Orbitrap mass analyzer, while successful integration with time-of-flight analyzers has already been demonstrated.

INTRODUCTION

Innovations in mass spectrometry (MS) instrumentation have had a sustained impact on the proliferation of MS technology and its widespread deployment in diverse areas of analytical research. The advent of soft ionization,[1−3] advancements in fragmentation methods,[4−9] and the development of high-performance mass analyzers[10−15] have established mass spectrometry as an indispensable tool in bioanalytical chemistry research. These extraordinary achievements are greatly facilitated by the development of powerful spectral interpretation and database search algorithms[16,17] as well as an impressive range of front-end separation techniques.[18−20] The demand for extended dynamic range, higher mass accuracy, and greater speed will continue to drive hardware developments and empower the analytical capabilities of MS instrumentation. Moreover, progress on fragmentation tools and methods are necessary to improve the analysis by MS of increasingly complex samples where molecular identification and fine structural or sequence information is required. The development of the Omnitrap platform addresses the demand for new MS technology with enhanced versatility and diverse

Received: July 29, 2022
Revised: September 8, 2022
Accepted: September 12, 2022
Published: September 16, 2022

applicability by integrating the entire arsenal of ion dissociation methods into a single instrument.

Radio-frequency (RF) quadrupole ion traps form one of the most multifaceted classes of analytical devices in the MS field. Since the conceptualization of this class of analyzers in the 1950s,[21] followed mainly by the development of the quadrupole mass filter,[22] RF ion traps have slowly evolved from items of curiosity to powerful analytical devices for tandem mass analysis (MS/MS) of molecular ions. Although the early endeavors were focused on understanding the properties and performance characteristics of the three-dimensional quadrupole ion trap (3D QIT),[23] attention gradually shifted toward the two-dimensional linear ion trap (2D LIT) configuration.[24]

RF ion trap technology has over half a century of accumulated development efforts to show, with a major focus on operating these devices as mass analyzers. The resonance detection technique[25] proposed originally for performing mass analysis with a three-dimensional quadrupole ion trap involved scanning the DC component to bring a frequency component of the ion motion in resonance with an auxiliary AC excitation signal. Limitations in the resolution and mass range inherent to this method were partially addressed by the introduction of the mass-selective instability method,[26] where sequential ejection of ions at the low-mass-cutoff instability was accomplished by ramping the amplitude of the RF waveform. Enhanced resolution over an extended mass range has been reported using the axial modulation technique involving the application of an auxiliary AC signal at the appropriate frequency.[27]

Mass separation based on the application of rectangular waveforms was first demonstrated experimentally on a quadrupole mass spectrometer by scanning amplitude, while the ability to generate a mass spectrum in the absence of a resolving DC component by using asymmetric waveforms was also highlighted.[28] The effect of finite rise/fall times on the mass resolving power were also simulated and rotations of the stability diagram by controlling duty cycle were demonstrated, while operation in the second stability zone have also been considered theoretically.[29] Extending the mass selective instability method to a 3D QIT device involves the application of an asymmetric rectangular waveform and performing a frequency scan instead.[30] The resonance ejection method performed at fixed α and q Mathieu parameters was also proposed, wherein the RF trapping field and an auxiliary AC dipole excitation field maintained at a selected fraction of the main RF frequency are scanned simultaneously.[31]

Today, the mass resolving power and mass accuracy typically offered by quadrupole ion traps is inferior to commercially available high-performance mass analyzers, such as Fourier-transform (FT) ion cyclotron resonance, Orbitrap, and time-of-flight. Despite this limitation, RF ion traps are undoubtedly the prominent choice for processing ions in the gas phase, primarily due to their inherent property to support an extensive range of ion activation-dissociation schemes and their unparalleled MS/MS capabilities. For example, the principles of photodissociation action spectroscopy were established using diffuse light sources[32] during the early development stages of ion trap technology. In addition, investigations concerned with ion−molecule reaction kinetics[33] initiated by electron ionization (EI), the determination of proton affinities in the gas phase,[34] the introduction of the kinetic method for acquiring information on thermochemical properties of molecular ions,[35,36] and structural characterization studies based on ion−molecule reactions[37] were early demonstrations of the versatility of quadrupole ion traps. Implementation of collision-induced dissociation (CID) by resonance excitation,[38] infrared multiphoton dissociation (IRMPD),[39] and surface-induced dissociation[40] were also demonstrated successfully in 3D quadrupole ion traps coupled to an EI source.

With the advent of electrospray ionization (ESI), enhanced performance IRMPD[41−43] of biomolecules was demonstrated in 3D quadrupole ion traps, and ultraviolet photodissociation (UVPD) experiments were also performed successfully for small peptides containing aromatic amino acids at 266 nm[44] and for chromophore-derivatized peptides at 355 nm.[45] Ion−ion reactions for charge state reduction involving proton transfer between opposite polarity ions have been performed successfully,[46] and the ion parking method to efficiently control the reaction rate and confine the reduced charge state envelope of protein mixtures within the available m/z range of the instrument has been demonstrated.[47] The first evidence for electron transfer in the gas phase involving multiply charged oligonucleotide anions formed by ESI and rare gas cations formed by EI was also obtained in a 3D QIT device.[48] Additionally, the use of the radical cations of fluoranthene was shown to dissociate phosphopeptide anions with fragments retaining the labile phosphorylation group and fewer neutral losses compared to xenon cations, an effect attributed to the lower ionization potential of fluoranthene and the corresponding lower recombination energy available in the reaction.[49] Charge inversion reactions[50] are yet another elegant example involving sequential ion-processing steps, highlighting further the remarkable versatility of RF trapping devices. Fragmentation methods developed in 3D QIT devices involving fast electrons and metastable or neutral radical species have also been described. Fragmentation reactions between negative ions of polypeptides and free electrons lead to dominant Cα−C fragmentation resulting predominantly in a$^{\bullet}$/x backbone fragments,[51] while fast atom bombardment by electronically excited noble gas species produced in a cold cathode discharge was shown to produce N−Cα, S−S bond cleavage, and Cα−C cleavage for peptide cations and anions, respectively.[52] Similarly, metastable atom-activated dissociation (MAD) was exercised by irradiating trapped ions with energetic beams of noble gases,[53] indicating the electron-mediated fragmentation character of this method and emphasizing the benefit for analyzing singly charged peptides. Phosphorylation sites were readily identified, and the differentiation of the isomeric leucine/isoleucine residues was made possible by a series of neutral losses from the side chains producing diagnostic w fragment ions. Determination of phosphorylation and sulfonation modifications in negative-ion mode have also been demonstrated successfully using this method.[54] The dissociation process involves Penning ionization in parallel with charge reduction of the protonated ions via electron capture. More recent fragmentation methods realized in a 3D QIT device include the hydrogen attachment/abstraction dissociation (HAD) of peptides using a heated tungsten capillary to dissociate molecular hydrogen.[55] The observed N−Cα bond cleavages leading to c/z$^{\bullet}$ type ions and the Cα−C bond cleavages leading to a$^{\bullet}$/x type ions were attributed to H$^{\bullet}$ attachment to the carbonyl oxygen and H$^{\bullet}$ abstraction from the peptide backbone, respectively. The technique was later extended to the structural analysis of phospholipids and the identification of the double bond position as well as the

https://doi.org/10.1021/jasms.2c00214
J. Am. Soc. Mass Spectrom. 2022, 33, 1990−2007

position of the acyl chains by reacting ions with hydroxyl radicals produced in a microwave-driven capacitively coupled plasma generator.[56] These experiments are refined examples highlighting the extensive diversification of RF ion trap designs and methods for dissociating ions, particularly when combined with high-level control of ion secular frequencies[57] enabling tandem mass spectrometry to be performed seamlessly.

Significant enhancements in injection efficiency and space charge capacity were accomplished with the introduction of linear quadrupole ion traps,[58,59] and particularly with the dual-pressure linear ion trap configuration dedicated to high throughput proteomics.[60,61] Experiments with 157 nm laser light highlighted the formation of a/x-type fragments in peptides and proteins[62] demonstrated facile disulfide bond cleavage in polypeptides,[63] while mechanistic studies to investigate salt bridge formation were also performed.[64] The development of electron-transfer dissociation (ETD),[65] concurrent with infrared photoactivation[66] or combined with higher energy collision dissociation (HCD)[67] are proven to be highly efficient methods for dissociating ions stored in 2D trapping devices. Implementation of the proton transfer approach combined with parallel ion parking for the analysis of mixtures of intact proteins[68] and UVPD of lipopolysaccharides,[69] singly charged peptides,[70] and proteins with 193 nm[71] and 213 nm photons combined with 10.6 μm CO_2 laser light[72] are additional examples of the analytical power of tandem MS based on 2D LIT systems. Notable are the developments of an off-axis linear ion trap for fast electron capture dissociation[73] and the branched RF ion trap for electron-based dissociation.[74] These advances in instrumentation and the corresponding fragmentation methods have had an extraordinary impact on the analysis of biomolecules by mass spectrometry.[75]

Less widely adopted but nonetheless highly informative fragmentation methods have been developed or implemented in 2D LIT systems. Photodissociation of iodo-tyrosine containing proteins by 266 nm photons generating a highly localized radical site on the aromatic ring of the modified tyrosine side chain and followed by collisional activation is shown to be a highly selective method for protein analysis.[76] Ionization and radical-driven dissociation of peptide cations induced via irradiation with helium ions in the keV energy range has also been reported.[77] Irradiation of proteins by energetic ions produced in a microwave air plasma source has also been explored, and the complex chemistry involving charge reduction effects via electron and proton transfer reactions between the colliding partners has been reported.[78] Single photon ionization by synchrotron VUV light has also been accomplished in an ion trap, and the threshold of ionization for different charge states of a protein has been measured with high precision.[79] Fragmentation of peptides via interactions with electronically excited metastable argon atoms have demonstrated the effectiveness of this method for analyzing singly charged ions and investigating post-translational modifications.[80] Finally, cryogenic ion spectroscopy combined with mass spectrometry is another exciting application enabled by ion trap technology providing new insights into peptide and protein structure.[81]

Radial confinement in ion traps is performed predominantly by sinusoidal RF waveforms applied to the pole electrodes at a fixed frequency and with variable amplitude. Despite the widespread use of LC oscillating circuits in commercial mass spectrometers, high power MOSFET switching technology employed to generate rectangular waveforms exhibits distinctive features, partly by enabling comprehensive control of the waveform properties. For example, an important advantage is the ability to control frequency over an extended range of values, thereby providing effective trapping windows over an extended range of mass-to-charge ratios that far surpasses those accessible by sinusoidal RF systems. Tandem MS experiments comprising the steps of ion isolation and CID via controlling the duty cycle of the rectangular waveforms have been demonstrated in a linear ion trap.[82] In addition, the "static" field established during trapping enabled by a flat-top waveform facilitates external injection of charged particles, and particularly electrons, with precise kinetic energy. Thus, successful implementation of ECD has been demonstrated in a 3D QIT device driven by a rectangular waveform,[83] and a ~0.5 s irradiation time was shown to provide ~5% conversion efficiency of peptides to fragments.

Variations of all the fragmentation methods discussed so far are implemented successfully in the Omnitrap platform. Design aspects of this novel linear ion trap and the exclusive multidimensional tandem MSn features of the technology are outlined below. The primary goal of this new device is to enable high-performance top-down MS by providing access to an extended ion activation network. The fragmentation toolbox available for designing MSn experiments comprises activation methods based on external injection of reagent ions, radical neutral species, photons, electrons, and also collisions with neutrals. The complementary information offered by these methods will enable in-depth characterization of biomolecular ions. Essential elements for supporting such a diverse ion activation network include: (a) a linear arrangement of 2D quadrupole segments connected in series for generating multiple trapping regions, with each trapping region dedicated to support a unique set of functions for processing ions, (b) a generator producing a pair of rectangular waveforms for radial ion confinement, providing access to mass-to-charge windows over an extended range while also permitting side injection of externally generated charged particles with precise kinetic energy, and (c) a system of pulse valves for tailoring pressure to the requirements of each of the individual steps performed in a tandem MS experiment. These three fundamental aspects of the design offer maximum flexibility for successful integration of the most comprehensive fragmentation toolbox in a single instrument.

Analytical figures of merit such as space charge capacity, ion isolation, and accumulation functionality are presented. Operation in MS2 and MS3 modes engaging the different ion activation methods available are demonstrated experimentally for protein ions. This first generation design of the Omnitrap platform is coupled to the Q-Exactive family of hybrid mass spectrometers (Thermo Fisher Scientific), greatly benefiting from the high mass resolving power, high mass accuracy, and extended dynamic range offered by the Orbitrap mass analyzer. Coupling of the Omnitrap platform to an ion mobility drift cell and an orthogonal time-of-flight mass analyzer has also been reported.[84]

INSTRUMENTATION

Design Features. The Omnitrap platform consists of nine consecutive quadrupole segments, labeled Q1−Q9 from entrance- to exit-end, arranged in a linear configuration and grouped to form three principal trapping regions for processing ions. The inscribed radius of the quadrupole field is 4.0 mm, and the length of each segment is customized to optimize the

https://doi.org/10.1021/jasms.2c00214
J. Am. Soc. Mass Spectrom. 2022, 33, 1990−2007

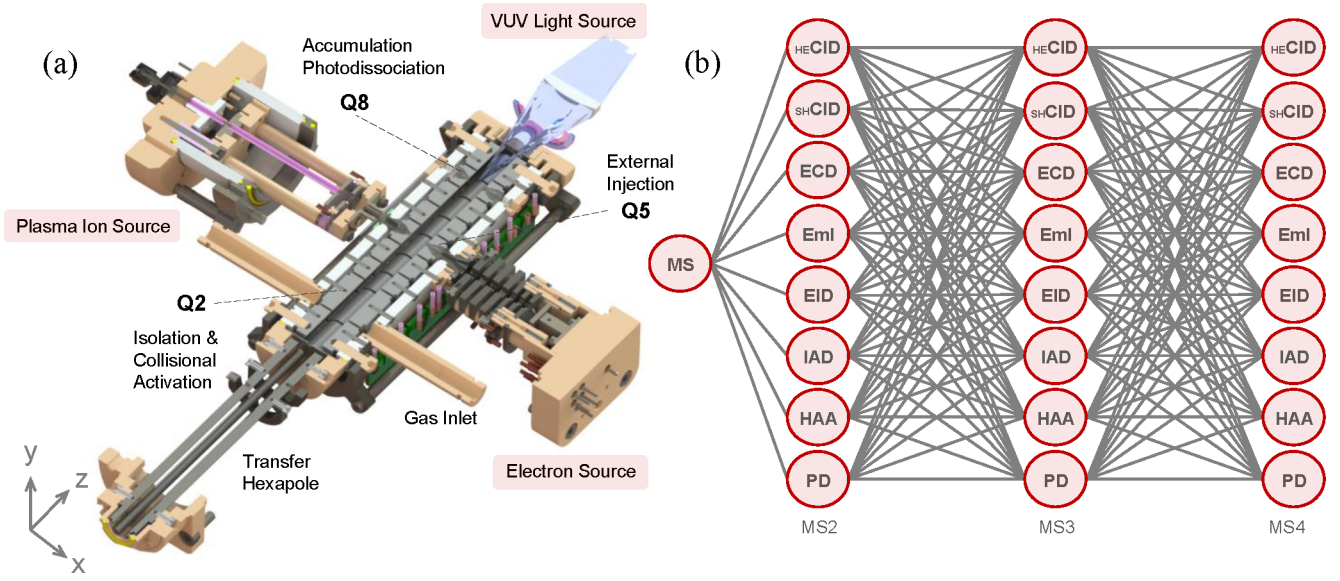

Figure 1. (a) Cross-sectional view of the Omnitrap platform highlighting the trapping regions designed for processing ions, external sources for injection of ions and electrons, inlets for pulsed gas injection, and the hexapole guide for transferring ions to and from an external source. (b) Ion activation network for multidimensional multiple-stage tandem MS workflows available in the Omnitrap platform. The ion activation network includes: higher energy collision-induced dissociation ($_{HE}$CID), slow-heating collision-induced dissociation ($_{SH}$CID), electron capture dissociation (ECD), electron meta-ionization (EmI), electron induced dissociation (EID), ion activated dissociation (IAD), hydrogen atom attachment (HAA), and photo-dissociation (PD).

diverse set of functions available throughout the ion trap volume. Fringe-fields induced by terminal lens-electrodes, axial squeezing, transfer and energy lift effects were all considered to define the optimum length of each segment. A frame-ring structure is designed to support ceramic platforms machined with pockets to position the quadrupole electrodes. The hyperbolic surface of the electrodes is wire-eroded to an accuracy of ~5 μm, while the overall construction is assembled with an accuracy of <20 μm. Truncation of the hyperbolic surfaces is balanced between minimizing the capacitive coupling between opposite RF phase electrodes and avoiding fringe field penetration into the trapping volume to obtain a more pure quadrupole field.

Gas pulses are admitted into the trapping volume through transfer tubes connected on the side ceramic platforms. A pressure level of $>10^{-2}$ mbar is maintained for ~20 ms during pulsed introduction of argon and nitrogen gases, while pressure relaxes to background levels (10^{-5} mbar) within a period of ~75 ms. A pair of pulse valves is employed for injecting gas pulses with a maximum repetition rate of 25 Hz.

Elevated pressure levels are desirable during axial injection of ions into the ion trap from an external source during collisional activation and for efficient thermalization of ions during their transfer between trapping regions. The ion trap volume is hermetically sealed using insulators inserted between the ceramic platforms, and differential pumping is provided by an 85 L/s turbomolecular pump.

Radial confinement of the ions is accomplished by a pair of opposite phase rectangular waveforms, typically operated at 250 V_{0p}. The frequency range of the waveforms extends from 100 kHz to 2.5 MHz, and phase-coherent frequency jumps to relocate ions in the α-q space can be performed throughout this frequency range. Ions are confined axially by switching DC voltages applied to individual segments. The number of DC levels made available to each segment during the course of an experiment is limitless, offering an unrestricted number of DC profiles that can be applied sequentially for axial transfer and processing of the ions. The DC signals are superimposed onto the RF component through an RC network with a time constant of 5 ms. Dipolar resonance excitation is available in segments Q2 and Q5 through the application of single frequency or notched AC waveforms to collisionally activate or select ions for tandem MSn workflows, respectively. Single precursor ion isolation is exercised by applying a resolving DC component to the pole electrodes of segments Q2 and Q5.

Figure 1a shows a cross-sectional view of the Omnitrap platform connected in series with a hexapole ion guide. An electron source and a plasma ion source attached symmetrically on either side of segment Q5 are used for external injection of charged particles for ion-particle reactions. Electrons and reagent ions are injected through 1.6 mm holes on the pole-electrodes of the quadrupole ion trap. Optical access is provided through 2.0 mm holes in segment Q8, as well as along the axis of the ion trap through a viewport disposed at the back-end of the device. A series of switches for controlling the DC levels is connected through 100 kΩ resistors, while the rectangular waveforms are transmitted through 10 nF capacitors. Auxiliary AC signals are superimposed to the rectangular waveforms using transformers with a ratio of 2:1. The Omnitrap platform is supplied with static and dynamic settings, which include variable frequency and DC signals, pulse valves, optical shutters, and trigger outputs for laser control. All static parameters are driven by microcontrollers and analogue subcircuits. An FPGA platform running at 100 MHz is developed to synchronize all the dynamic settings applied to the ion trap. The control software is developed in C#, and fast communication is accomplished using USB3 technology.

Ion Activation Network. The underlying design principle of the Omnitrap platform is to efficiently integrate existing fragmentation techniques and to provide a versatile architecture for the development of new ion-processing tools and

https://doi.org/10.1021/jasms.2c00214
J. Am. Soc. Mass Spectrom. 2022, 33, 1990−2007

tandem MSn protocols. The ion activation network supported by the current design is presented in Figure 1b. The Omnitrap platform appears particularly suitable for top-down characterization of proteins where different activation−dissociation methods can be applied selectively to design advanced multidimensional multiple-stage analytical workflows. Nevertheless, the extended ion activation−dissociation network also offers new directions for standard high-throughput experiments where, for example, EID can be exercised on liquid chromatographic time scales with high efficiency.

Slow heating CID using multiple excitation frequencies in resonance with precursor ions distributed over different charge states is available in segments Q2 and Q5 in the x and y directions, respectively. Slow heating CID in ion traps driven by rectangular waveforms applied with a fixed amplitude utilize frequency jumps to park ions of interest at the desired q_z value in the stability diagram. Consequently, the depth of the effective potential remains fixed throughout the mass range of interest,[85] in contrast to the effective potential increasing with mass-to-charge as a result of the higher RF amplitude applied when sinusoidal waveforms are employed for trapping ions. Phase space simulations of resonance excitation can easily illustrate the more energetic excursions of ions trapped by rectangular waveforms, and any limitations imposed on the CID efficiency of high m/z ions due to the shallow effective potential may be counterbalanced by an enhancement in the rate of vibrational excitation and/or a reduction in the number of soft collisions providing thermalization. Although these effects remain largely unexplored, highly efficient slow heating CID has been demonstrated experimentally for intact monoclonal antibodies[86] with the trapping voltage of the rectangular waveforms set to 250 V_{0p}, suggesting that the depth of the effective potential is not a practical limitation.

In addition, beam-type CID is implemented by transferring ions from one trapping segment to another along the axis of the ion trap with kinetic energies of >10 eV. The degree of acceleration is controlled by the gradient of the DC profile established across neighboring segments. Precursor and products ions may subsequently undergo efficient deceleration within a uniform quadrupole field instead of experiencing the strong defocusing action when a stopping potential is applied to a terminal lens electrode, which is typically associated with heavy ion losses, especially in the higher kinetic energy regime. Slow heating and beam-type CID are performed during a gas pulse transient permitting high level of control and optimization of these processes.

Electron-based dissociation is enabled by the application of rectangular waveforms to the electrodes of the quadrupole ion trap creating "static field" conditions during trapping. Side injection then becomes possible since even at the frequencies considered, and electrons travel fast enough to reach the ion cloud before the polarity of the rectangular waveform is switched. In the current design, the power supply driving the hot filament can be floated up to 1 kV negative potential relative to the DC offset applied to segment Q5, corresponding to a maximum kinetic energy available in ion-electron reactions of 1 keV. The ability to scan the energy range of externally injected electrons allows ion-electron interactions to be investigated from the low energy regime (∼0 eV) where electron capture is efficiently accomplished to the higher energy regime where electron meta-ionization (EmI) and electron induced dissociation (EID) phenomena are observed. EmI in particular leads to the detachment of one or more electrons from (de)protonated ions producing stable radical species, which offers a unique opportunity for investigating fundamental aspects of the rich ion chemistry manifested in radical driven dissociation processes and also for enhancing sequence coverage.

In addition to the mainstream CID and ExD excitation methods available in the Omnitrap platform, fragmentation based on ion activation dissociation (IAD) has also been implemented successfully. A dielectric barrier discharge is established in the form of a plasma jet, producing an energetic beam of ions transmitted through the storage region of the quadrupole ion trap. The plasma medium currently employed is hydrogen gas and a high-density beam of a mix of H^+, H_2^+, and H_3^+ ions is used for ion activation dissociation. Experiments with small- to medium-size proteins presented below are shown to produce rich fragmentation spectra, with all types of primary fragment ions observed, characterized by strong meta-ionization and charge reduction effects.

Viewports located on either side of segment Q8 and through the back end of the device allow photodissociation experiments to be performed. Simultaneous or sequential irradiation with two laser sources is therefore readily available. Axial injection of lasers also allows for photoactivated ExD experiments to be executed directly in segment Q5. The ion activation network presented in Figure 1b can therefore be envisaged in three dimensions where two different ion-activation techniques can be applied simultaneously. Another such example is collisionally activated ECD, enabled by an auxiliary AC signal delivered to segment Q5.

Depending on the requirements of the application, methods where different activation-dissociation steps are applied sequentially to maximize the information output may be required, particularly in top-down analysis where in-depth characterization of intact proteins is pursued. For example, a first MS2 CID step to generate a smaller number of high-intensity fragments followed by MS3 ECD of selected fragments may produce mass spectra with high S/N, postprocessing of which is exceedingly more reliable compared to confronting a highly congested MS2 ECD or MS2 UVPD spectrum. Another example may involve electron meta-ionization to generate multiply protonated radical ions, which can be subsequently subjected to MS3 CID, producing significantly more informative mass spectra. In this context, the Omnitrap platform provides a unique framework for navigating through a multidimensional ion activation network, tailoring different sequential activation-dissociation steps to the application and optimizing the analysis of increasingly complex samples.

Methods for Advanced Ion Processing. Axial transfer of ions is enabled by DC switching potentials producing weak gradients between trapping regions. Typically, axial transfer is preceded by an energy lift step to raise ion potential energy in the source trapping region above the DC level of the receiving trapping region. This two-step process eliminates losses observed when the transition of the DC profile is switched in a single step between two distinct trapping regions. An example utilizing all three trapping regions involving the steps of ion isolation in Q2, EmI in Q5, ion accumulation in Q8, and ultimately MS3 CID of radical ions in Q2 is shown in steps (a)−(g) of Figure 2.

In more detail, ions received from an external source are thermalized in segment Q2 and the $[M+nH]^{n+}$ ions are isolated either by the application of a resolving DC component

https://doi.org/10.1021/jasms.2c00214
J. Am. Soc. Mass Spectrom. 2022, 33, 1990−2007

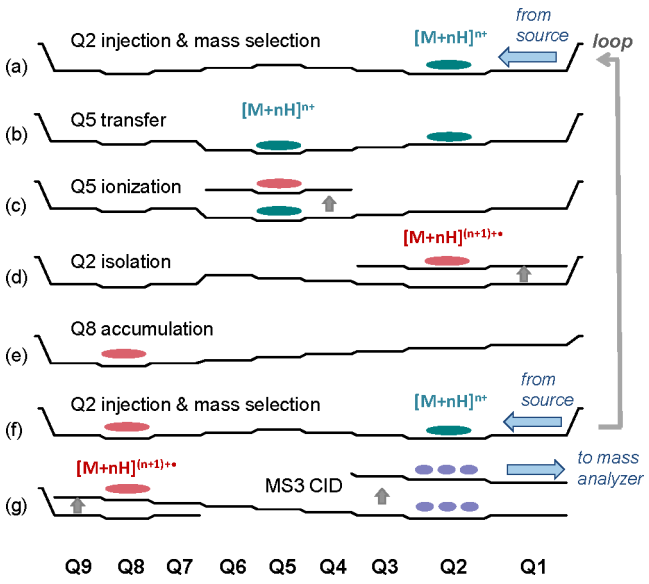

Figure 2. Transitions of the axial DC profile applied across the ion trap in a multiple-stage tandem MS experiment including the steps of Q2 injection and ion isolation (a), Q5 transfer (b) followed by electron meta-ionization (c), Q2 ion isolation of meta-ionized species (d), Q8 transfer and accumulation (e), Q2 loop injection (f) and Q2 collisional activation of accumulated population and fragment ion ejection (g).

or a multifrequency notched waveform (a). The initial DC profile receiving ions in Q2 is designed with an additional trapping region in segment Q8. Leakage of ions to the Q8 trapping region during injection in Q2 is prevented by a potential barrier established across segments Q4−Q6. Precursor ions are subsequently transferred from Q2 to Q5 (b), and ion potential energy is raised to generate the desired potential difference between the trapping region and the potential applied to the hot filament (c). Ionization of multiply protonated ions via irradiation with fast electrons is optimized to maximize production of the radical species $[M+nH]^{(n+1)+\bullet}$ with minimal EID-type fragmentation. The entire population is transferred back to Q2 for mass selection of the radical ions (d), which are subsequently transferred and stored in the accumulation segment Q8 (e). The cycle is completed by switching back to the original DC profile for receiving a new packet of ions from the external source (f). The maximum number of loops is dictated by the space charge capacity of the accumulation region, while the space charge limit can be increased by unifying segments Q7−Q9. Limitations in the maximum number of ions that can be processed may also be imposed by space charge effects during processing in different trapping regions of the Omnitrap platform. In this example, the enriched population of the $[M+nH]^{(n+1)+\bullet}$ radical ions is transferred and rethermalized in segment Q2 (g). MS3 slow heating CID is accomplished by dipolar excitation using a single frequency component corresponding to the secular frequency of the ions. Energy lift is finally applied to define the kinetic energy of the ions during the ejection process.

Electron Source and Optics. Electrons are produced by direct heating (6 A) of a 1.6 mm diameter tantalum disk cathode supported on a ceramic disk (Kimball Physics, US). The heating current source is floated on two separate power supplies, an operational amplifier for precise control at the lower electron energy regime (0 to 150 eV) and a low-ripple high-voltage power supply (−1.0 kV) for generating high kinetic energy electrons. A high voltage reed relay is used to switch between the two modes. A fast operational amplifier is driving a split lens-electrode between deflection and focusing potentials to enable external injection of electrons in segment Q5 over a predetermined period of time, facilitating synchronization of the ExD functionality with the event sequence applied during the course of an experiment. A stack of lens-electrodes optimized by simulations is used for extracting electrons from the hot cathode. An additional set of split lens-electrodes is employed for effective steering of the electron beam to correct for misalignment between the source and segment Q5.

Figure 3 shows a SIMION[87] model and electron trajectories simulated under space charge conditions. In this example,

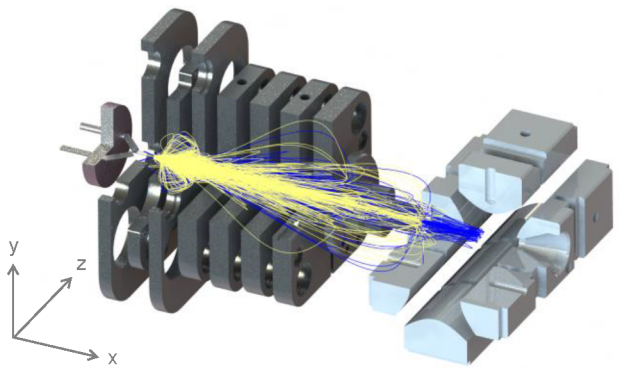

Figure 3. SIMION model of the electron optics illustrating external injection of electrons in segment Q5. Low energy electrons are admitted in the ion trap during the positive phase of the rectangular waveform applied to the side quadrupole-electrode (blue trace) and reflected during the negative phase (yellow trace).

electrons are admitted into the ion trap with the lowest possible energy, arriving at the center of the quadrupole field with practically 0 eV kinetic energy (blue trace). Also shown are the trajectories of electrons deflected by the negative phase of the rectangular waveform applied to the side pole-electrode of the quadrupole ion trap (yellow trace). The 2D static quadrupole field creates a strong focusing effect for low energy electrons in the vertical direction (y-axis) and simultaneously defocuses the beam along the axis of the ion trap (z). This is a very convenient condition for maximizing the overlap between externally injected electrons and an axially elongated ion cloud confined by the DC potentials applied to neighboring segments of Q5.

The electron beam is monitored on a lens electrode across segment Q5 and the current available for ExD is estimated in the range of ∼1.0 μA. Greater electron currents can be measured only when the kinetic energy of the electrons is raised above 500 eV, thus reducing the space charge and improving transmission through the 1.6 mm aperture on the side quadrupole electrode.

Plasma Jet Ion Source. Ions stored in segment Q5 can also be irradiated by a dense beam of ions produced in a plasma jet. The beam is injected into the trapping volume through a focusing lens and a 1.6 mm aperture on the pole-electrode. The plasma source shares a common axis with the electron source and consists of a conductive tube in series with a ceramic tube forming a uniform flow domain for transferring plasma ions to the quadrupole ion trap. A DC bias is applied to

https://doi.org/10.1021/jasms.2c00214
J. Am. Soc. Mass Spectrom. 2022, 33, 1990−2007

the conductive part of the tube and a dielectric barrier discharge is initiated when a gas pulse raises pressure inside the flow domain to submbar levels. The energy of the charged particles entrained in the free jet expansion is approximately equivalent to the magnitude of the voltage applied to initiate the discharge (≥1 kV).

The plasma jet was characterized in a separate rig using a set of DC lenses and a quadrupole mass filter (m/z 1−200) in a coaxial arrangement. Molecular hydrogen was admitted through a gas inlet system incorporating a pulse valve and a leak valve. Dense beams of hydrogen ions, H^+, H_2^+, and H_3^+, were obtained over a wide range of voltage settings and pressures. The stopping potential method was employed and a ± 200 eV kinetic energy spread was measured for ∼1 keV ions.

Under pulsed operation of the plasma jet ion source with the maximum repetition rate of 12 Hz, pressure in the vacuum chamber of the Omnitrap platform was maintained below 10^{-4} mbar. The maximum residence time of hydrogen ions injected through the ion trap and monitored using a fast oscilloscope is ∼5 ms, while a peak current of ∼5 μA was measured across segment Q5. In the MS2 experiments presented here, hydrogen ions were injected through segment Q5 with ∼1 keV kinetic energy.

Vacuum Ultraviolet Light Source. A continuous polychromatic, high-brightness vacuum ultraviolet (VUV) light source with emission maxima at around 120 and 160 nm (Hamamatsu, Germany) was also integrated in the Omnitrap platform. The lamp is connected on a flange using bellows to provide flexible penetration inside the vacuum chamber. The diffuse light is focused near the trapping region of segment Q8 with a MgF_2 planoconvex lens (Korth, Germany). The diameter of the lens is 50 mm, and the radius of the curvature was adjusted to 42.3 mm producing a focal length of 100 mm for 200 nm photons. Since the refractive index of MgF_2 is a function of wavelength, focusing of polychromatic light is not ideal. Nevertheless, the ability to displace the light source and also control the position and/or the length of the ion cloud along the axis of the ion trap provides reasonable flexibility to optimize the fragmentation process.

A free-standing, vacuum-compatible optical shutter (Vincent Associates, US) is installed in between the MgF_2 lens and a 2.5 mm aperture lens-electrode adjacent to segment Q9. The stainless-steel S-blades of the shutter are designed with an aperture size of 25.4 mm and can be operated in continuous mode at 10 kHz. The shutter control is synchronized with the event sequence applied to the ion trap in order to inject light over a predetermined time window.

VUV photodissociation using a diffuse light source must be exercised with care due to the high number of photoelectrons produced inside the ion trap. For the Omnitrap configuration, capture of photoelectrons is considered a low probability fragmentation channel due to the acceleration of the electrons by the trapping field. Fragment ions other than those produced by photon absorption can be attributed to interactions with fast electrons, similarly to EID. Nevertheless, the defocusing action of the trapping field is expected to reduce such contributions to fragmentation and the effect can be minimized further by the application of a strong DC gradient along the axis of the ion trap pulling electrons away from the region where ions are stored. The application of high negative potential to the lens electrode adjacent to Q9 was used to reduce the background ion signal observed in the mass spectrum.

Thermal Cavity H• Source. An incandescent cavity source has been developed for producing a thermal beam of hydrogen atoms[88] to investigate hydrogen atom attachment (HAA) reactions. A high current power supply is used for direct heating of tantalum or tungsten thin-wall cavities. The cavities are typically 5 cm long and constructed with a <2.0 mm internal diameter. A pulse valve delivers consecutive pulses of molecular hydrogen in-through the hot cavity. Cracking of molecular hydrogen to generate hydrogen atoms occurs on the tantalum surface maintained at 1400 °C or on tungsten at 1600 °C. The mixture of H_2 and $H^•$ species is injected into the trapping volume through an aperture on the side quadrupole electrode. Pressure transients are similar to those established during operation of the plasma ion source where a maximum pressure of $>10^{-2}$ mbar is reached for a period of ∼5 ms. The thermal cavity source has two mounting positions and injection of hydrogen atoms is possible either in segment Q5 or in segment Q8. Fragmentation of proteins via interactions with thermal hydrogen atoms is an inefficient process; however, attachment reactions occur readily and may offer new insights into fragmentation mechanisms and intramolecular hydrogen atom rearrangement reactions.

Mass Spectrometry. The Omnitrap platform was coupled to two different mass spectrometers, the Q Exactive Plus and the Q Exactive HF. On both instruments, the electrometer located at the back of the HCD-cell was removed, and an RF transfer hexapole was installed to allow for ion transport to the Omnitrap platform. Additionally, each mass spectrometer is equipped with modified, research-grade software that enables lossless ion transport to and from the segmented linear ion trap prior to mass analysis. The coupling of the Omnitrap system to the Orbitrap mass spectrometers lowers the acquisition rate due to the additional ion-processing time. The shortest ion-processing time within the Omnitrap in MS2 mode is typically 50 ms, including the transfer time to and from the device, which in turn limits the acquisition speed of the mass spectrometer to ∼10 Hz. In tandem MSn experiments where multiple-stages are employed, the ion-processing cycle can increase to the second time scale. All spectra are generated with the mass resolving power of the Orbitrap analyzer set to 140,000 (fwhm) at m/z = 200. The number of scans used for averaging is adjusted to reach a signal-to-noise ratio of $>10^5$.

EXPERIMENTAL SECTION

Sample Preparation and ESI. Ubiquitin from bovine erythrocytes (≥98% purity) and ammonium acetate were purchased from Sigma Chemical Co. (St. Louis, MO, USA). Acetic acid and HPLC-grade water were obtained from Fisher Scientific (Leics, UK). All reagents were used without further purification. Two 10 μM solutions were prepared by dissolving ubiquitin in either aqueous 1% acetic acid or in 100 mM ammonium acetate aqueous solution, corresponding to the partially unfolded (charge states 7+ and 8+) and the native protein conformations (charge states 5+ and 6+), respectively. Papaverine hydrocloride (99%) was purchased from ACROS Organics and a 0.1 mM stock solution was prepared in ACN/H_2O/AcOH 90:10:0.1 (v/v/v). A series of dilutions were performed to final concentrations of 0.003, 0.03, 0.15, and 0.3 μM in order to map the stability diagram of the Omnitrap under different space charge loads. Bradykinin acetate salt (≥98%) was purchased from Sigma-Aldrich, and 1.2 μM

https://doi.org/10.1021/jasms.2c00214
J. Am. Soc. Mass Spectrom. 2022, 33, 1990−2007

solution was prepared in H_2O/MeOH/AcOH 60:39:1 (v/v/v) in order to measure the secular frequency of the ions under variable space charge loads and across a wide range of excitation amplitudes. Oxidized insulin chain B from bovine pancreas (≥80%) and myoglobin from equine heart were purchased from Sigma-Aldrich. Insulin chain B 10 μM solution was prepared in ACN/H_2O/AcOH 50:49.9:0.1 (v/v/v) and 10 μM myoglobin solution was prepared in H_2O/MeOH/AcOH 49:49:2 (v/v/v).

Data Analysis. Data processing was performed with a new data processing tool developed in-house (Fasmatech), using the MS-Product (Protein Prospector) online fragment calculator modified to include multiply charged internal b- and a-type ions. Theoretical isotopic distributions of ubiquitin fragment ions were generated using the enviPat web 2.4 calculator (Swiss Federal Institute of Aquatic Science and Technology). New algorithms were developed to fit the calculated isotopic distributions to ubiquitin fragmentation mass spectra based on multiple score functions in order to maximize the confidence in the assignments. The deconvolution step was eliminated in this new data processing workflow due to the high number of errors associated with the identification of monoisotopic masses in highly congested spectra. External mass calibration was applied using high-intensity ubiquitin fragments and all assignments were performed with a mass accuracy of ±6 ppm.

RESULTS AND DISCUSSION

Stability Diagram: Space Charge Capacity. Mapping of the stability diagram was performed experimentally by scanning the frequency of the rectangular waveforms, Ω, and the amplitude of the resolving DC component, V_{DC}, to displace ions in $\alpha - q$ parameter space. The stability parameters are functions of the frequency, Ω, the mass-to-charge ratio of a given species and the inscribed radius of the quadrupole ion trap, r_o. namely: $\alpha = 8\ eV_{DC}/(mr_o^2\Omega_o^2)$ and $q = -4\ eV_{rect}/(mr_o^2\Omega_o^2)$. The stability diagram is generated for singly protonated papaverine ions (m/z = 340.15) stored in segment Q2 under variable space charge loads and a fixed rectangular waveform amplitude of V_{rect} = 250 V_{0p}. Ions are selected in the quadrupole mass filter of the Q Exactive MS and the duration of the storage period in Q2 for all the $\alpha - q$ coordinates explored is set to 20 ms. In these experiments the frequency range of the rectangular waveform is scanned from 780 kHz to 2.4 MHz.

Figure 4 shows the stability diagram and the ion losses attributed to space charge effects determined experimentally by injecting ∼0.5 M charges into the Omnitrap platform. Characteristic islands of instability are identified where the ion signal is reduced by 20% at $q > 0.5$ and across the entire range of α values. Greater losses are observed as the storage period is increased, while near-complete loss of the ions is observed in these regions of the stability diagram when >2 M charges are stored in segment Q2. While the vertical instability observed at $q \sim 0.51$ will not interfere strongly with many operations performed in the ion trap, for example, during injection or collisional activation at lower q values, the efficiency of ion isolation based on the resolving DC method will be compromised when ions are parked at the tip of the stability diagram and the instability occupies an even greater area in the $\alpha - q$ parameter space as the space charge load is increased. Ion losses are no longer observed below 50,000 charges. The stability diagram of the Omnitrap platform

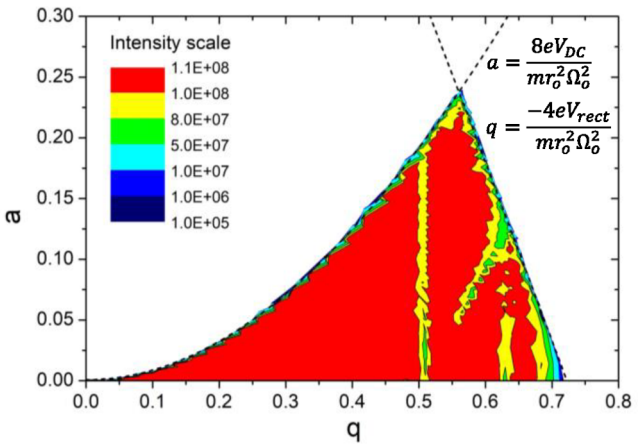

Figure 4. Stability diagram and ion losses attributed to space charge effects measured experimentally for ∼0.5 M charges injected in the Omnitrap platform and stored in segment Q2 for 20 ms. The theoretical boundaries of the first stability region are shown with dashed lines.

determined experimentally is in good agreement with the theoretical boundaries of the first stability region.[89]

Secular Frequency: Calibration. An elaborate procedure is developed to take into account the shifts in ion secular frequency induced by variable space charge loads and differences in the amplitude of the AC dipolar excitation signal. Dipolar resonance excitation is performed in the presence of pulsed argon gas to enable high efficiency slow heating CID. An example of the strong shifts in the secular frequency observed for bradykinin $[M+2H]^{2+}$ ions is provided in the Supporting Information (Figure S1). The calibration procedure requires generating a large set of data points for different space charge loads and excitation amplitudes. In the first step, secular frequency is plotted as a function of the number of charges for the lowest excitation amplitude where CID fragments are generated. The "primary" secular frequency ω_0 is obtained at the lowest space charge load and corresponds closely to the value calculated theoretically for linear ion traps driven by rectangular waveforms.[90] In the second step, a linear fit across the data points corresponding to the lowest excitation amplitudes is used to determine the slope and, together with ω_0, provide an estimation of ω_1, which corresponds to the new secular frequency dictated by the space charge load. The additional shift is determined by plotting secular frequency as a function of excitation amplitude for the same data set to obtain a new slope, and together with ω_1, provide an estimation of ω_2, which corresponds to the actual secular frequency dictated by both the space charge load and by the excitation amplitude. This calibration process is performed across a wide m/z range for ions with different charge states and the overall accuracy is calculated to be ±0.2 kHz. This calibration procedure is expected to enhance information produced in data-dependent acquisition workflows, where vastly different densities of ions across a wide m/z range are subjected to collisional activation or isolation processes.

Ion Isolation. Ion isolation in the Omnitrap platform is performed in segments Q2 and Q5 using three different schemes. The first scheme is equivalent to the method employed in quadrupole mass filters where a resolving DC component is applied to the pole electrodes of the ion trap. Trapped ions are placed at the tip of the stability diagram for a

https://doi.org/10.1021/jasms.2c00214
J. Am. Soc. Mass Spectrom. 2022, 33, 1990−2007

period of ~1 ms. A single region of the mass spectrum can be isolated, and the resolution of ion isolation is limited to 100 across a wide mass range. The second scheme is based on the application of dipolar excitation frequency sweep waveforms designed with a single or multiple notches. Isolation windows with a resolution of ~200 can be generated using 10 ms long waveforms. Higher resolution can be obtained using the third scheme where the same sweep waveform designed with a wider notch is applied twice, while a shift in the frequency of the rectangular waveforms is utilized to displace ions within the notch. This latter scheme can increase the resolution of isolation to >400 with the rectangular waveform amplitude fixed at 250 V_{0p}.

The experimentally calculated resolution for the three different schemes obtained in segment Q2 and across a wide m/z range is presented in the Supporting Information (Figure S2). The ions subjected to ion isolation were generated by MS2 CID of ubiquitin $[M+5H]^{5+}$. Figure 5a shows a region of

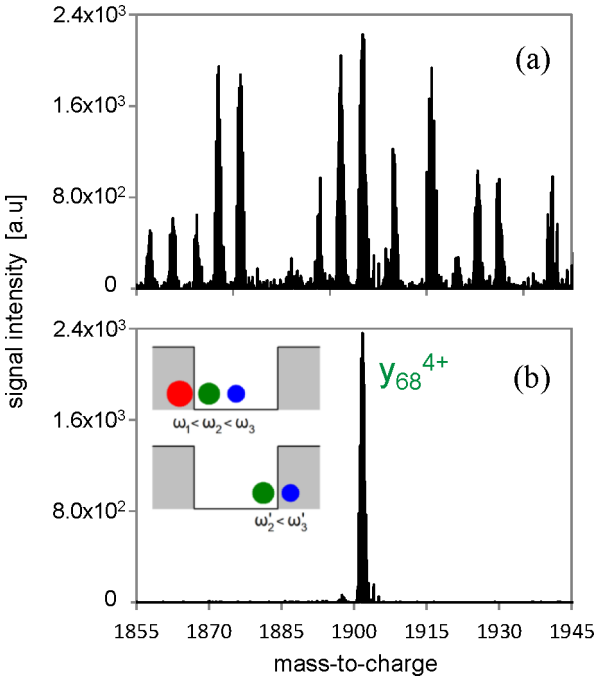

Figure 5. (a) Part of the MS2 CID mass spectrum of ubiquitin $[M+5H]^{5+}$ and (b) the y_{68}^{4+} fragment ions isolated by performing a frequency jump in ion secular frequency between the application of the two consecutive sweep waveforms.

the MS2 CID spectrum of ubiquitin while Figure 5b shows the y_{68}^{4+} fragment ions selected with a resolution of >400. The illustration in Figure 5b also highlights the ion secular frequency jump induced by a shift in the frequency of the rectangular waveforms applied between the first and second frequency sweeps.

Collision-Induced Dissociation. The slow heating MS2 CID spectrum of the partially unfolded[91] ubiquitin charge state $[M+8H]^{8+}$ shown in Figure 6 is generated by dipolar excitation in the presence of an argon gas pulse for a period of 10 ms. Slow heating CID is performed by adjusting frequency to 975 kHz to park ions at q = 0.15 with low mass cutoff of 225 Th. Extensive and sequential fragments from the N-terminal-half of the protein are observed, with y-type fragments dominating the mass spectrum. This is in contrast to the more disfavored fragments from the C-terminal-half of the protein, a pattern observed for all the different charge states examined. Despite the relatively nonspecific fragmentation of the intermediate charge states of ubiquitin, and particularly for the $[M+8H]^{8+}$ charge state examined here, a few dominant dissociation channels can be identified. The most abundant fragments are generated by backbone cleavages next to proline residues 19 and 37, while abundant fragment ions are also observed on the C-terminal side of aspartic acid residues 32, 39, and 52. Neutral losses of H_2O and NH_3 are also observed with high abundance. The fragmentation patterns observed in the CID mass spectrum of the $[M+8H]^{8+}$ charge state generated in the Omnitrap platform are consistent with previous studies investigating slow heating CID of ubiquitin in a three-dimensional QIT trap.[92]

The CID spectrum is processed manually, and the fragment search was limited to a-, b-, and y-type ions including H_2O and NH_3 neutral losses from these fragments. The sequence coverage obtained for the $[M+8H]^{8+}$ ions of ubiquitin is 72% (a = 19%, b = 48%, and y = 69%). The total ion intensity assigned including neutral losses is 94%, with y-type fragments comprising the majority of the ion signal (79%). The remaining unassigned 6% of the total ion intensity in the CID mass spectrum can be attributed to internal fragments and also to primary fragments with side chain losses.

Electron-Activated Dissociation. External injection of electrons is performed in segment Q5 where ion-electron interactions extending from the low energy range promoting electron capture to the high energy range for radical ion formation via ionization and electron induced dissociation are established with high efficiency. The electron current available for ion activation−dissociation in the current design is on the order of ~1 μA and scales with the kinetic energy of the electrons. The lowest kinetic energy of the electrons available in reactions with stored ions is determined by the potential difference between the hot cathode and the DC potential in the center of Q5, while the kinetic energy spread is dictated by the trapping parameters (effective potential) and particularly by space charge that ultimately defines the size of the ion cloud.

The different reaction regimes observed in the lower energy range are provided in Figure 7 where the $[M+3H]^{3+}$ insulin chain B species are exposed to electrons with kinetic energies ranging between 0 and 50 eV. The different regimes corresponding to electron capture, hot electron capture and electron ionization can be clearly distinguished with the corresponding optimum energies identified at 0 eV, 7 and 35 eV. The onset of the meta-ionization process is observed at ~12 eV, while the tailing effects observed for "negative" kinetic energy electrons is attributed to the increased volume occupied by the ion cloud at lower q values and the wider kinetic energy spread available in reactions with electrons. The reactions leading to hydrogen abundant and hydrogen-deficient ions in ECD and EID respectively, and corresponding mass spectra, are shown in the Supporting Information (Figure S3). The separation obtained between the electron capture and the hot electron capture regimes becomes less apparent in experiments with ubiquitin; however, the optimum electron energies remain identical.

Electron-detachment dissociation (EDD) experiments on DNA molecules have also been performed successfully in negative-ion mode, with a maximum efficiency of ionization-

https://doi.org/10.1021/jasms.2c00214
J. Am. Soc. Mass Spectrom. 2022, 33, 1990−2007

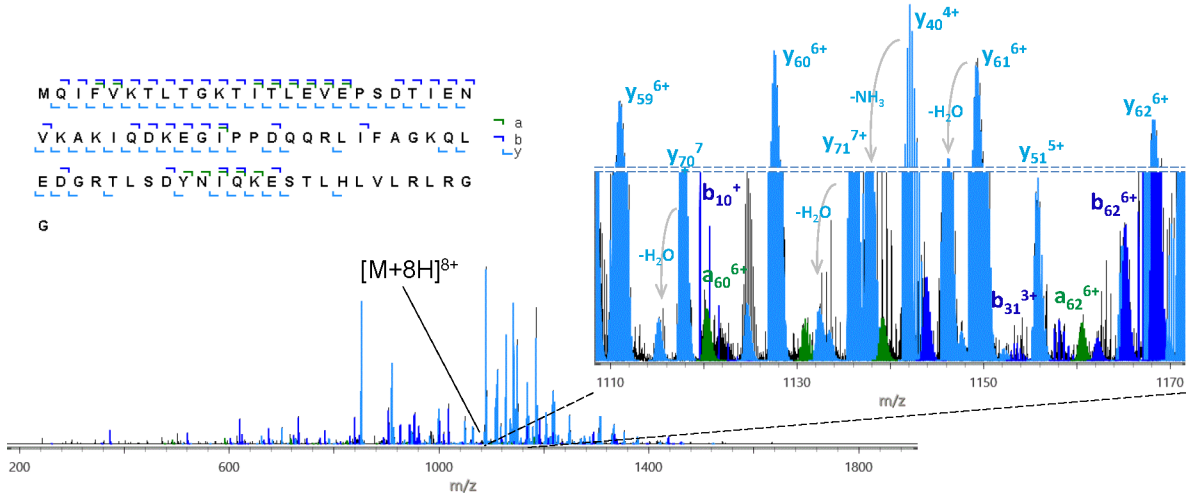

Figure 6. Annotated slow heating CID mass spectrum of ubiquitin $[M+8H]^{8+}$ ions performed in Q2 and b-y fragment sequence map. The mass spectrum is generated by averaging the ion signal over ∼150 scans.

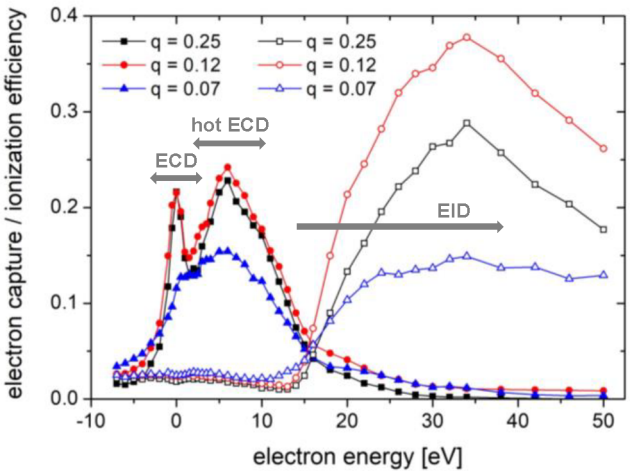

Figure 7. Electron capture (0−20 eV) and ionization efficiency (>12 eV) as a function of electron kinetic energy for insulin chain B $[M+3H]^{3+}$ ions, highlighting the ECD, hot ECD, and EID regimes.

dissociation observed at 35 eV, similarly to EID in positive ion mode.

In EmI the conversion of even electron $[M+nH]^{n+}$ species to the hydrogen-deficient radical ions, $[M+nH]^{(n+1)+\bullet}$, appears to be a more efficient reaction compared to ECD where fragments are generated by the charge-reduced hydrogen-abundant species, $[M+nH]^{(n-1)+\bullet}$, especially as the kinetic energy of the electrons is increased to 1 keV. In both cases, exposing protein ions to electrons will lead to dissociation with ECD and EID fragments differing in the number of hydrogen atoms and charge state (Figure S4).

Ubiquitin has been used extensively as a benchmark protein to evaluate the efficiency of different fragmentation methods and complete sequence coverage has been reported for the 11+ charge state by ECD.[93] Figure 8a shows the annotated ECD mass spectrum and the corresponding sequence map highlighting the complete sequence coverage obtained for charge state 8+ in the Omnitrap platform. The abundant fragmentation observed for the $[M+8H]^{8+}$ ions in ECD is explained by the much less ordered conformation compared to the lower charges states of the protein.[94] Figure S5 shows ECD primary fragment ion intensities and the corresponding charge state distribution plots. The ECD mass spectrum of ubiquitin $[M+8H]^{8+}$ ions is generated by injecting electrons with an energy of <5 eV and within a time window of 150 ms. All types of primary fragment ions are being formed, with $c/z^{\bullet}$ fragments generated throughout the backbone except next to proline residues, covering 96% of the amino acid sequence. A significant number of y-type fragments are also formed providing 91% sequence coverage, while additional information throughout the backbone is obtained by the remaining a- (77%), x- (55%), and b-type (25%) fragments. The formation of b- and y-type fragments can be explained by the ejection of a H atom from the charge reduced hydrogen-abundant $[M+8H]^{7+\bullet}$ species to form even electron precursor ions.[95] The complementarity relationship reported for $a^{\bullet}/y$ high-intensity fragment pairs in ECD of doubly and triply charged tryptic peptides[96] is also observed here. The assignments including primary fragments, H_2O, NH_3 losses and charge reduced ECD precursor ions account for 84% of the total ion signal. Additional identifications corresponding to d, v, w and a/b internal fragments raise the assignments to 86% of the total ion intensity, with c-type fragments comprising the majority of the ion signal (23.4%), followed by z (21.6%), a (10.2%), y (9.1%), x (2.0%), and b (1.9%). 95% of ubiquitin peptide bonds are cleaved by at least one complementary fragment pair, with c−z pairs exhibiting the maximum complementarity (89%). The complementary pair c_{59}^{5+}/z_{17}^{2+} exhibits the highest intensity in the ECD spectrum,[97] which is also in agreement with previous studies performed with selected conformers of the 8+ charge state.[98]

Figure 8b shows the annotated EID mass spectrum of ubiquitin $[M+8H]^{8+}$ ions. Figure S6 provided in the Supporting Information also shows EID primary fragment ion intensities and the corresponding charge state distribution plots. Fragments are generated by irradiating ions with a ∼ 2 μA, 35 eV electron beam over a period of 100 ms. Complete sequence coverage is obtained for the 8+ charge state, while, consistent with early investigations in EID of ubiquitin 7+ charge state ions,[99] all types of primary fragment ions are being formed. The a-type fragments cover 92% of the amino acid sequence, followed by x = 88%, z = 85%, c = 77%, y = 72%, and b = 53% ions.

https://doi.org/10.1021/jasms.2c00214
J. Am. Soc. Mass Spectrom. 2022, 33, 1990−2007

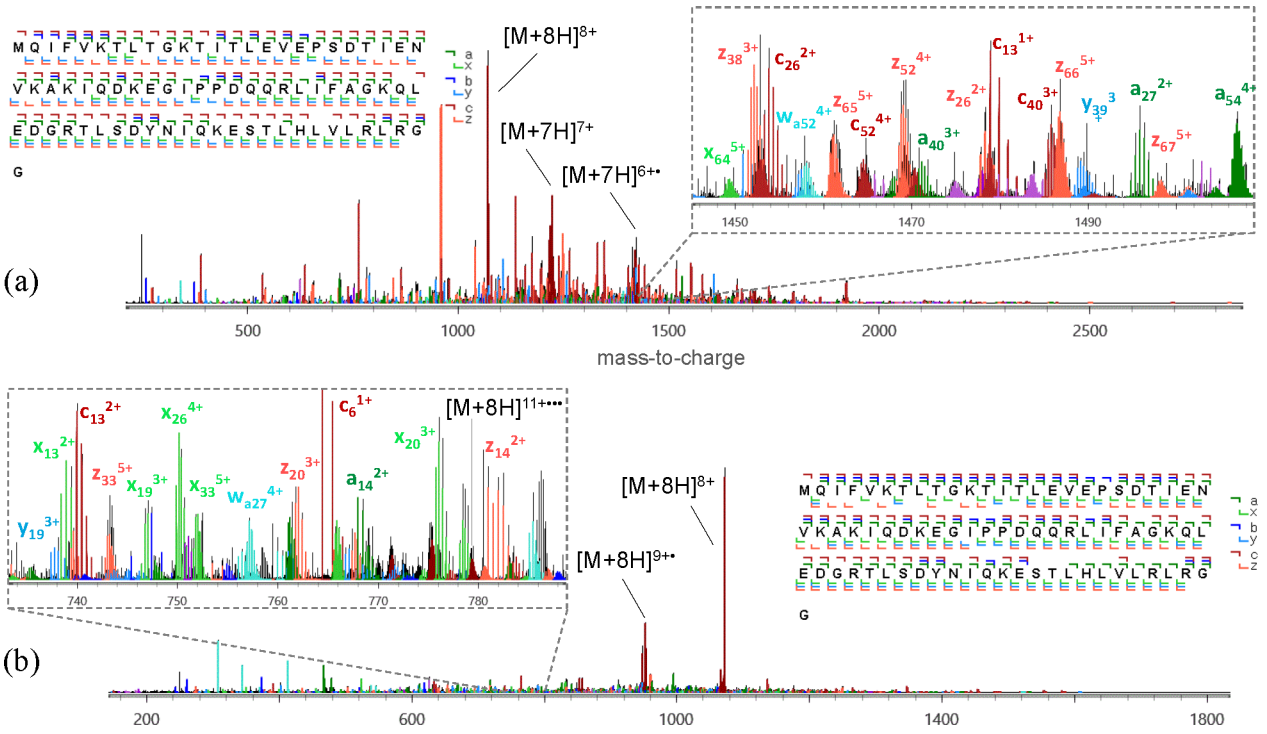

Figure 8. (a) Annotated MS2 ECD mass spectrum of ubiquitin generated by exposing the $[M+8H]^{8+}$ ions to ~1 μA electron current for 150 ms in segment Q5. Complete sequence coverage is obtained with c/z$^{\bullet}$ fragments covering 96% of the amino acid sequence. (b) Annotated MS2 EID mass spectrum of ubiquitin generated by exposing the $[M+8H]^{8+}$ ions to ~2 μA electron current for 100 ms in segment Q5. Complete sequence coverage is obtained, with a-type fragments providing 92% sequence coverage and comprising 13.5% of the total ion signal. The mass spectra are generated by averaging the ion signal over ~500 scans.

The overall EID complementarity (92%) is similar to ECD, although in this case the a−x pair shows the highest contribution (80%). The assignments including primary fragments, H_2O, NH_3 losses, and the ionized EID precursor ions account for 74% of the total ion signal. Additional d, v, w, and a/b internal fragments raise the assigned signal to 79%, with a-type fragments comprising the majority of the ion signal (13.5%), followed by z (9.3%), x (8.6%), c (7.5%), y (6.6%), and b (4.8%).

Neutral side-chain losses are also observed in the form of d, v, and w ions, which are generated for more than half of the total number of amino acids of the protein. Diagnostic d and w ions were assigned confirming the position for 3 of 7 isoleucine residues, while additional w_a ions were identified confirming another 7 of 9 leucine residues present in the sequence.

Compared to EID, ECD produced fewer diagnostic d and w ions that can be used to distinguish between leucine from isoleucine residues. Another characteristic feature in EID is the loss of the CO_2 group, either from the C-terminus or from acidic residues, observed for the irradiated precursor $[M+8H]^{8+}$ ions as well as for all intermediate meta-ionized radical species, $[M+8H]^{9+\bullet}$ and $[M+8H]^{10+\bullet\bullet}$. Multiple CO_2 losses are observed as the electron energy is increased to the maximum level available in the current setup (~1 keV), while the extent of ionization is enhanced over fragment ion formation leading to even higher charge state ions, $[M+nH]^{(n+k)(k\times\bullet)}$, where n is the number of protons and k the number of electrons detached from the protein ($k \leq 4$ for 300 ms reaction time).

Hydrogen Ion Activated Dissociation. The annotated HIAD mass spectrum of ubiquitin $[M+8H]^{8+}$ ions is shown in Figure 9a. Figure S7 provided in the Supporting Information shows HIAD primary fragment ion intensities and the corresponding charge state distribution plots. Injection of a ~ 1 keV pulsed hydrogen ion beam in the ion trap comprising predominantly of H^+ and H_2^+ species leads to meta-ionization of the isolated 8+ precursor charge state via detachment of one or more electrons, in a process similar to EID. A series of charge-reduced precursor ions is also generated, closely resembling the hydrogen abundant intermediate product ions typically observed in ECD/ETD. Careful examination of the isotopic distributions of the charge-reduced ubiquitin ions shows that proton abstraction is an additional mechanism involved in product ion formation, albeit this reaction pathway is less favored compared to meta-ionization and charge-reduction via electron capture.

Charge-reduced ions are found to be more abundant compared to the ionized intermediate species; however, in time-resolved experiments the intensity of the ionized hydrogen-deficient ions at the onset of the reaction is greater, suggesting that meta-ionization precedes charge reduction. Therefore, a likely source of the free electrons driving charge reduction is the detachment of low energy electrons in meta-ionization of ubiquitin by hydrogen ions, a process similar to electron ionization dissociation described for peptides and proteins.[99,100] The formation of negative ions from background impurities cotrapped in Q5 and acting as electron donors is a less favored explanation for the formation of the charge reduced intermediates due to the prompt extraction of these ions by the axial field designed for storing positive ions only. These observations imply that fragments are formed by two parallel radical driven mechanisms, namely, electronic excitation followed by electronic-to-vibrational energy transfer similar to EID, and charge-reduction following the capture of low energy electrons, similar to ECD. Complete sequence

https://doi.org/10.1021/jasms.2c00214
J. Am. Soc. Mass Spectrom. 2022, 33, 1990−2007

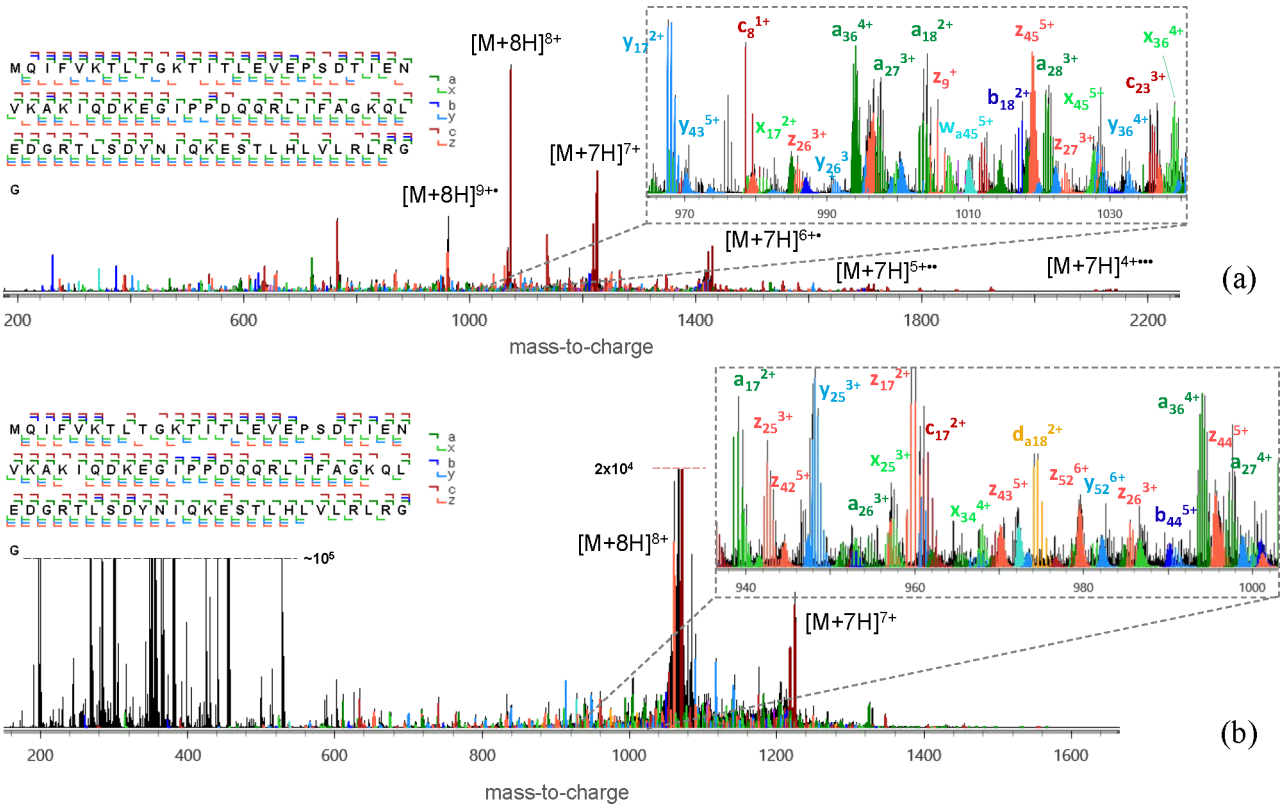

Figure 9. (a) Annotated MS2 HIAD mass spectrum of ubiquitin generated by exposing the $[M+8H]^{8+}$ ions to ∼1 keV atomic and molecular hydrogen ions in segment Q5 for ∼10 ms over a storage period of 400 ms. Complete sequence coverage is obtained, with z-type fragments providing 81% sequence coverage and comprising 13.4% of the total ion signal. (b) Annotated VUVPD mass spectrum of ubiquitin generated by exposing the $[M+8H]^{8+}$ ions to polychromatic light emitted from a deuterium lamp for a period of 500 ms. Complete sequence coverage is obtained with the a/x fragment pairs exhibiting 97% sequence coverage and 75% complementarity. The HIAD mass spectrum is generated by averaging the ion signal over ∼40 scans and the UVPD spectrum over ∼150 scans.

coverage is obtained for the 8+ ubiquitin charge state with all types of primary fragment ions being formed throughout the backbone, as shown in Figure 9a.

The z-type fragments cover 81% of the amino acid sequence, followed by a = 80%, x = 76%, c = 76%, y = 75%, and b = 24% ions, while 84% complementarity was achieved (c−z = 63%).

The assignments including primary fragments, H_2O, NH_3 losses, and the ionized precursor ions account for 81% of the total ion signal. Additional d, v, w, and a/b internal fragments raise the assigned signal to 83%, with c-type fragments comprising the majority of the ion signal (13.8%), followed by z (13.4%), a (10.1%), y (8.9%), x (4.6%), and b (4.2%). Although d, v, and w ions represent only ∼1% of the ion signal, 44% of leucine residues can be distinguished by the w_a diagnostic ions. Multiple neutral side chain losses are observed on aspartic acid and threonine, indicating their participation in radical driven dissociation pathways. Comparable results have been produced in top-down experiments with myoglobin, and 92% sequence coverage is obtained (Figure S8). The results produced in HIAD of ubiquitin and myoglobin bear similarities with experiments using helium ions accelerated to higher kinetic energies (4−10 keV) and recently extended to other reagent gases, including hydrogen.[101] It was established that the ionization energy of the projectile atomic ions has a negligible effect on the activation of biological ions; thus, resonance charge transfer was ruled out as a possible activation mechanism. The term electronic stopping has been used instead, to describe the electronic excitation of target biomolecules induced by fast projectile ions through the so-called long-range ion-electron interactions, providing higher excitation energies with interaction times on the femtosecond time scale.[102] Electron capture was also considered in parallel to electronic stopping to explain the different fragmentation pathways of peptides, comprising mostly of low m/z amino acid side chains and immonium ions, whereas the signal from larger m/z fragments and backbone scission products was largely suppressed. The rich fragmentation mass spectrum presented in Figure 9a for the 8+ charge state of ubiquitin providing complete sequence coverage can be explained, at least in part, by the high density hydrogen ion beam produced in the plasma jet ion source.

VUV Photodissociation. The annotated VUV photodissociation mass spectrum of ubiquitin $[M+8H]^{8+}$ ions is shown in Figure 9b. Figure S9 provided in the Supporting Information shows VUVPD primary fragment ion intensities and the corresponding charge state distribution plots. All types of primary fragment ions are generated providing complete sequence coverage of the intact protein, despite the lower fragmentation efficiency of the $[M+8H]^{8+}$ precursor ion compared to experiments with electrons and hydrogen ions. The a/x fragment pairs are the most abundant species in the mass spectrum, while y ions located next to proline residues 19, 37, 38 and a c ion next to aspartic acid residue 39 are the most abundant fragments in the mass spectrum. The x-type fragments cover 87% of the amino acid sequence, followed by a = 85%, c = 68%, y = 67%, z = 65%, and b = 25% ions, while

https://doi.org/10.1021/jasms.2c00214
J. Am. Soc. Mass Spectrom. 2022, 33, 1990−2007

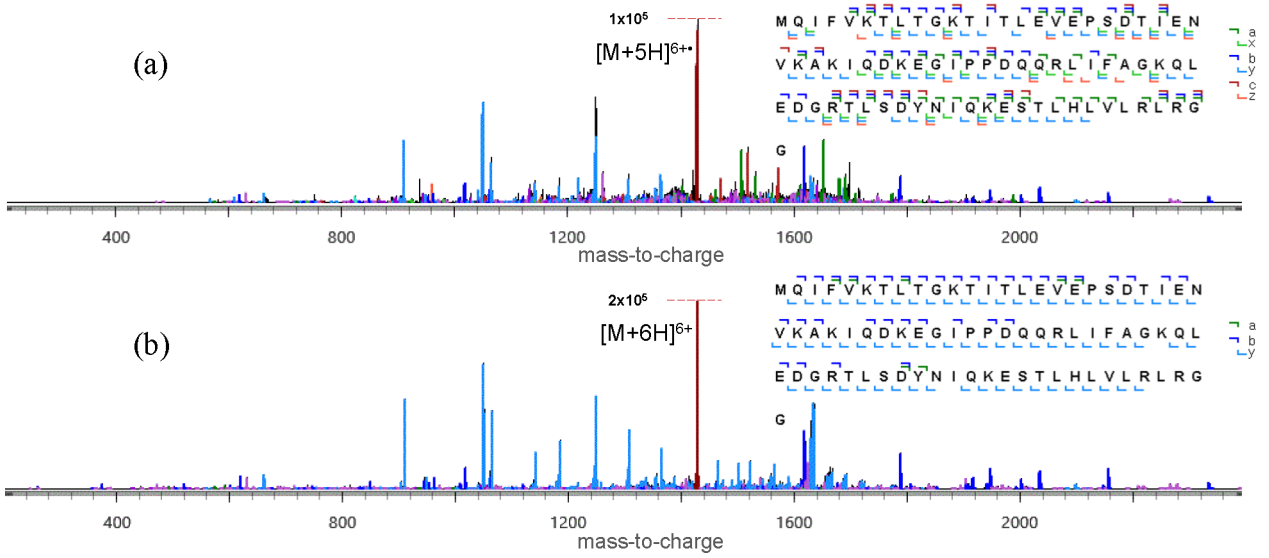

Figure 10. (a) Annotated MS3 CID mass spectrum and corresponding sequence map of hydrogen-deficient ubiquitin $[M+5H]^{6+\bullet}$ radical ions produced in Q5 by irradiation of the 6+ charge state by 35 eV electrons. (b) Annotated MS2 CID mass spectrum and corresponding sequence map of even electron ubiquitin $[M+6H]^{6+}$ ions produced in the ESI source. The mass spectra are generated by averaging the ion signal over ~100 scans.

84% complementarity was achieved, mainly due to a−x complementary pair (75%). The assignments including primary fragments, H_2O, and NH_3 losses account for 25% of the total ion signal. Additional d, v, and w fragments raise the assigned signal to 26%, with a-type fragments comprising the majority of the ion signal (4.5%), followed by x (2.9%), z (2.8%), c (2.6%), y (2.6%), and b (0.6%). 44% of leucine and 57% of isoleucine residues can be distinguished by d and w diagnostic ions. Extensive side chain losses arise from most aspartic acid residues (4/5), as well as threonine (4/7) and serine residues (2/3). The absence of the charge reduced $[M+8H]^{7+\bullet}$ species from the mass spectrum (only the $[M+7H]^{7+}$ ions are detected as a result of proton abstraction by background impurities present in the HCD cell) is an indication that photoelectrons produced during injection of the VUV light in the ion trap are not involved in the ion activation-dissociation process. This is in contrast to experiments performed with the same deuterium light source coupled to a linear ion trap where charge reduction of proteins as a result of electron capture was observed and irradiation times as long as 30 s were necessary to dissociate peptides in positive ion mode.[103] The VUVPD mass spectrum presented in Figure 9b is generated by irradiating ions in Q7 for a period of 500 ms. Extending the period of irradiation has no effect on the fragmentation efficiency of ubiquitin.

MS3 CID of Radical Protein Ions in Accumulation Mode. The conversion efficiency of any given charge state of ubiquitin $[M+nH]^{n+}$ to the meta-ionized species $[M+nH]^{n+\bullet}$ using 35 eV electrons is approximately 20%. The efficiency with which radical ions are generated via detachment of electrons is enhanced further as the kinetic energy of electrons or the size of proteins is increased. The assumption that heavier proteins can redistribute the vibrational energy imparted via electronic excitation following electron impact may explain the ability of these ions to maintain their stability. EID fragmentation is suppressed in reactions with higher kinetic energy electrons where multiple electrons can be detached from proteins to generate multiradical ion species. EID fragmentation is promoted over ionization as the period of interaction is increased. The structure of the proteins is yet another factor that will influence the degree of ionization and the extent of fragmentation. For example, up to four electrons have been detached in experiments with singly protonated insulin generated by matrix-assisted laser desorption ionization without an appreciable amount of fragmentation, presumably due to the extensive disulfide bond network of the protein.[104] In contrast, the majority of singly charged peptides investigated so far appear to undergo EID fragmentation, with only a small fraction of those producing the doubly charged radical cations in low abundance.[105]

The ability to detach with high efficiency electrons from polyprotonated proteins provides a powerful tool to investigate the nature of these radical ions by exploring hydrogen atom rearrangements or electron hole propagation and recombination effects, or to simply enrich fragmentation and enhance sequence coverage and complementarity for low charge state proteins. An example of a top down experiment with radical protein ions is illustrated in Figure 10a where the 5+ charge state of ubiquitin is meta-ionized to form the hydrogen-deficient $[M+5H]^{6+\bullet}$ radical ions, which are subsequently subjected to MS3 CID. The results produced for the $[M+5H]^{6+\bullet}$ ions are contrasted to MS2 CID of the even electron $[M+6H]^{6+}$ ions presented in Figure 10b.

For the $6^{+\bullet}$ ions, additional b-type fragments are formed near the C-terminus and new b-type cleavages are observed next to lysines 29 and 63, phenylalanine 45, threonine 55, serines 57 and 65, and glutamic acid 63. The intensity of the y_{22} fragment next to threonine 55 is also enhanced considerably compared to MS2 CID. All new c/z and a/x ions generated from the radical hydrogen-deficient precursor are located next to aromatic residues, threonines, serines, acidic, and basic residues. These preferential dissociation pathways were also observed in MS3 CID experiments with the $8^{+\bullet}$ and $12^{+\bullet}$ ubiquitin radical ions. A possible mechanism explaining the new cleavages observed experimentally is the migration of the electron hole to a neutral basic site, initiating a cascade of intramolecular hydrogen atom rearrangements leading to fragmentation.[106] Residues carrying a hydroxyl

https://doi.org/10.1021/jasms.2c00214
J. Am. Soc. Mass Spectrom. 2022, 33, 1990−2007

group on the side chain can serve as a source of hydrogen atoms, leaving behind a neutral radical site $-O^{\bullet}$ that initiates radical driven dissociation. The extensive side chain fragmentation observed in experiments with insulin $4^{+\bullet}$ ions are a characteristic example of the rich chemistry observed in the dissociation of radical ions.[107]

The signal-to-noise levels achieved in MS3 CID of ubiquitin 6+• ions are equivalent to those obtained in MS2 CID of the 6+ species. This is accomplished by operating the Omnitrapplatform in accumulation mode, described in more detail with reference to Figure 2. Figure S10 shows the additional number of ions stored in each scan and summed in up to 50 cycles. A quasi-linear growth of the accumulated population is observed until segment Q8 is filled with approximately 2 M charges. The charge accumulation rate declines beyond this threshold due to the excessive space charge present in the ion trap. The capacity of the Omnitrap platform to accommodate ions can be extended further by combining neighboring segments to form a longer trapping region for storing and processing an even greater number of ions.

CONCLUSIONS AND OUTLOOK

The design of the Omnitrap platform can be considered as a first genuine attempt to integrate the entire fragmentation toolbox established to date into a single unit and alleviate limitations for processing ions in the gas phase. The main objective is to enhance the characterization of intact biomolecules by top down MS, especially the larger systems where utilization of the diverse ion activation network can generate complementary information. Examples of the complementary nature of different fragmentation methods such as EID, ECD and UVPD for the structural and functional characterization of larger proteins have been discussed.[108]

The capacity of the Omnitrap platform to empower top down MS is demonstrated by the complete sequence coverage achieved for ubiquitin 8+ charge state with four different fragmentation methods involving electrons, photons and reagent ions. The degree of complementarity accomplished in these experiments can only be approached by UVPD[109] and AI-ETD.[110] Despite the low intensity fragments observed in experiments driving precursor ions against the surface of the pole-electrodes under dipolar excitation conditions and in the absence of a buffer gas, high efficiency surface-induced dissociation (SID) remains the only method yet to be implemented. This implementation will be explored further by placing an SID surface at the far end of segment Q9.

The ion accumulation functionality is another critical aspect of the design where MSn workflows can be realized with high efficiency, particularly suited for top down experiments where the extensive number of dissociation channels produces low abundance fragment ions. An example of an MS3 experiment with ubiquitin radical ions is presented to demonstrate the unique capability of the Omnitrap platform in preserving signal-to-noise levels at the expense of duty cycle.

The enhanced versatility and extended capabilities of the Omnitrap platform come hand-in-hand with increased complexity and a number of ensuing complications, which have been carefully addressed. One example is the high-intensity background ions observed in the lower m/z region in VUVPD of ubiquitin, which are considerably more abundant compared to the background ion signal observed in EID and occupy a significant fraction of the space charge accommodated in the ion trap. Improvements in the design of the Omnitrap have been finalized and outgassing of unsatured hydrocarbons from polyether−ether−ketone (PEEK) material responsible for the enhanced background ion signal has been eliminated. Furthermore, to address the complexity of the instrument control software, a new simplified graphical user interface has been developed, facilitating the design of complex experimental workflows considerably. An extended library of standardized experiments has also been developed, which can be customized further based on user-specific analytical requirements.

The ExD data on ubiquitin are generated by electrostatic focusing of electrons in Q5, whereas ongoing experiments with ring magnets incorporated in the design enhance collimation of the electron beam further, improve robustness and show an improvement in the speed of ExD by a factor of 5×. Currently, data dependent acquisition MS2 EID experiments can be performed successfully using 35 ms ion-electron reaction times, and efforts in this direction are expected to improve ExD performance further. Fast EID reactions available on liquid chromatographic time scales are expected to play an important role for the analysis of small molecules and low charge state ions.

Enhancements in the resolution of ion isolation will be afforded with the new rectangular waveform generator currently being tested at 800 V_{0p}. The ion-processing arsenal is presently being expanded to include a source of fast neutral radicals, as well as ion mobility drift cell enabling MSn-IMS experiments. Integration of the Omnitrap platform with the next generation Exploris Orbitrap mass spectrometers has been completed successfully, expanding the adaptability of the device further. Finally, the combination of such a variety of fragmentation methods qualifies the Omnitrap platform as an excellent tool for exploring the gas-phase chemistry of ions across a wide mass range.

ASSOCIATED CONTENT

Supporting Information

The Supporting Information is available free of charge at https://pubs.acs.org/doi/10.1021/jasms.2c00214.

Experimental results, primary fragment ion intensity and charge state distribution plots, MS2 HIAD of myoglobin and corresponding sequence map, enrichment of the ion population as a function of the number of loop scans (PDF)

AUTHOR INFORMATION

Corresponding Author

Dimitris Papanastasiou − *Fasmatech Science & Technology, TESPA Lefkippos, NCSR Demokritos, Agia Paraskevi, 15341 Athens, Greece;* orcid.org/0000-0003-2299-9479; Email: dpapanastasiou@fasmatech.com

Authors

Diamantis Kounadis − *Fasmatech Science & Technology, TESPA Lefkippos, NCSR Demokritos, Agia Paraskevi, 15341 Athens, Greece*

Alexandros Lekkas − *Fasmatech Science & Technology, TESPA Lefkippos, NCSR Demokritos, Agia Paraskevi, 15341 Athens, Greece*

Ioannis Orfanopoulos − *Fasmatech Science & Technology, TESPA Lefkippos, NCSR Demokritos, Agia Paraskevi, 15341 Athens, Greece*

https://doi.org/10.1021/jasms.2c00214
J. Am. Soc. Mass Spectrom. 2022, 33, 1990−2007

Andreas Mpozatzidis − *Fasmatech Science & Technology, TESPA Lefkippos, NCSR Demokritos, Agia Paraskevi, 15341 Athens, Greece*
Athanasios Smyrnakis − *Fasmatech Science & Technology, TESPA Lefkippos, NCSR Demokritos, Agia Paraskevi, 15341 Athens, Greece;* orcid.org/0000-0003-1677-4214
Elias Panagiotopoulos − *Fasmatech Science & Technology, TESPA Lefkippos, NCSR Demokritos, Agia Paraskevi, 15341 Athens, Greece*
Mariangela Kosmopoulou − *Fasmatech Science & Technology, TESPA Lefkippos, NCSR Demokritos, Agia Paraskevi, 15341 Athens, Greece*
Maria Reinhardt-Szyba − *Thermo Fisher Scientific, 28199 Bremen, Germany*
Kyle Fort − *Thermo Fisher Scientific, 28199 Bremen, Germany*
Alexander Makarov − *Thermo Fisher Scientific, 28199 Bremen, Germany;* orcid.org/0000-0002-7046-6709
Roman A. Zubarev − *Department of Medical Biochemistry and Biophysics, Karolinska Institutet, 17165 Solna, Sweden;* orcid.org/0000-0001-9839-2089

Complete contact information is available at: https://pubs.acs.org/10.1021/jasms.2c00214

Notes

The authors declare no competing financial interest.

■ ACKNOWLEDGMENTS

The authors would like to acknowledge the support by the European Union Horizon 2020 research program under grant agreement 829157 (TopSpec FET project).

■ REFERENCES

(1) Fenn, J. B.; Mann, M.; Meng, C. K.; Wong, S. F.; Whitehouse, C. M. Electrospray Ionization for Mass Spectrometry of Large Biomolecules. *Science* **1989**, *246*, 64−71.
(2) Tanaka, K.; Waki, H.; Ido, Y.; Akita, S.; Yoshida, Y.; Yoshida, T.; Matsuo, T. Protein and polymer analyses up to m/z 100 000 by laser ionization time-of-flight mass spectrometry. *Rapid Commun. Mass Spectrom.* **1988**, *2*, 151−153.
(3) Karas, M.; Hillenkamp, F. Laser Desorption Ionization of Proteins with Molecular Masses exceeding 10,000 Da. *Anal. Chem.* **1988**, *60*, 2299−2301.
(4) Papayannopoulos, I. A. The Interpretation of Collision-Induced Dissociation Tandem Mass Spectra of Peptides. *Mass Spectrom. Rev.* **1995**, *14*, 49−73.
(5) Wells, J. M.; McLuckey, S. A. Collision-Induced Dissociation (CID) of Peptides and Proteins. *Methods Enzymol.* **2005**, *402*, 148−185.
(6) Zubarev, R. A. Reactions of Polypeptide Ions with Electrons in the Gas Phase. *Mass Spectrom. Rev.* **2003**, *22*, 57−77.
(7) Lermyte, F.; Valkenborg, D.; Loo, J. A.; Sobott, F. Radical Solutions: Principles and Application of Electron-based Dissociation in Mass Spectrometry-based analysis of Protein Structure. *Mass Spectrom. Rev.* **2018**, *37*, 750−771.
(8) Brodbelt, J. J.; Morrison, L. J.; Santos, I. Ultraviolet Photodissociation Mass Spectrometry for Analysis of Biological Molecules. *Chem. Rev.* **2020**, *120*, 3328−3380.
(9) Stiving, A. Q.; VanAernum, Z. L.; Busch, F.; Harvey, S. R.; Sarni, S.; Wysocki, V. H. Surface-Induced Dissociation: An effective Method for Characterization of Protein Quaternary Structure. *Anal. Chem.* **2019**, *91*, 190−209.
(10) Marshall, A. G.; Hendrickson, C. L.; Jackson, G. S. Fourier Transform Ion Cyclotron Resonance Mass Spectrometry: A Primer. *Mass Spectrom. Rev.* **1998**, *17*, 1−35.
(11) Hendrickson, C. L.; Quinn, J. P.; Kaiser, N. K.; Smith, D. F.; Blackney, G. T.; Chen, T.; Marshall, A. G.; Weisbrod, C. R.; Beu, S. C. 21 T Fourier Transform Ion Cyclotron Resonance Mass Spectrometer: A National Resource for Ultrahigh Resolution Mass Analysis. *J. Am. Soc. Mass Spectrom.* **2015**, *26*, 1626−1632.
(12) Hecht, E. S.; Scigelova, M.; Eliuk, S.; Makarov, A. Fundamentals and Advances of Orbitrap Mass Spectrometry. Encyclopedia of Analytical Chemistry: Applications, Theory and Instrumentation. *Mass Spectrometry* **2019**, x DOI: 10.1002/9780470027318.a9309.pub2.
(13) Beck, S.; Michalski, A.; Raether, O.; Lubeck, M.; Kaspar, S.; Goedecke, N.; Baessmann, C.; Hornburg, D.; Meier, F.; Paron, I.; Kulak, N. A.; Cox, J.; Mann, M. The Impact II, a Very High-Resolution Quadrupole Time-of-Flight Instrument (QTOF) for Deep Shotgun Proteomics. *Mol. Cell. Proteom* **2015**, *14*, 2014−2029.
(14) Chernushevich, I. V.; Merenbloom, S. I.; Liu, S.; Bloomfield, N. A W-Geometry Ortho-TOF MS with High Resolution and up to 100% Duty Cycle for MS/MS. *J. Am. Soc. Mass Spectrom.* **2017**, *28*, 2143−2150.
(15) Giles, K.; Ujma, J.; Wildgoose, J.; Pringle, S.; Richardson, K.; Langridge, D.; Green, M. A Cyclic Ion Mobility-Mass Spectrometer System. *Anal. Chem.* **2019**, *91*, 8564−8573.
(16) Chen, C.; Hou, J.; Tanner, J. J.; Cheng, J. Bioinformatics Methods for Mass Spectrometry-Based Proteomics Data Analysis. *Int. J. Mol. Sci.* **2020**, *21*, 2873.
(17) Halder, A.; Verma, A.; Biswas, D.; Srivastava, S. Recent Advances in Mass Spectrometry-Based Proteomics Software, Tool and Databases. *Drug Discov. Today Technol.* **2021**, *39*, 69−79, DOI: 10.1016/j.ddtec.2021.06.007.
(18) Zhang, Y.; Fonslow, B. R.; Shan, B.; Baek, M. C.; Yates, J. R., III Protein Analysis by Shotgun/Bottom-up Proteomics. *Chem. Rev.* **2013**, *113*, 2343−2394.
(19) Yi, L.; Piehowski, P. D.; Shi, T.; Smith, R. D.; Qian, W. J. Advances in Microscale Separations towards Nanoproteomics Applications. *J. Chromatogr. A* **2017**, *1523*, 40−48.
(20) Gomes, F. P.; Yates, J. R., III Recent Trends of Capillary Electrophoresis - Mass Spectrometry in Proteomics Research. *Mass Spectrom. Rev.* **2019**, *38*, 445−460.
(21) Paul, W.; Steinwedel, H. A New Mass Spectrometer without a magnetic field. *Z. Naturforsch.* **1953**, *8a*, 448−450.
(22) Dawson, P. H. Quadrupole Mass Analyzers: Performance, Design and Some Recent Applications. *Mass Spectrom. Rev.* **1986**, *5*, 1−37.
(23) March, R. E. Quadrupole Ion Traps. *Mass Spectrom. Rev.* **2009**, *28*, 961−989.
(24) Douglas, D. J.; Frank, A. J.; Mao, D. Linear Ion Traps in Mass Spectrometry. *Mass Spectrom. Rev.* **2005**, *24*, 1−29.
(25) Paul, W.; Steinwedel, H. Apparatus for Separating Charged Particles of Different Specific Charges. US Patent 2,939,952, 1960.
(26) Stafford, G. C., Jr.; Kelley, P. E.; Syka, J.E. P.; Reynolds, W. E.; Todd, J.F. J. Recent Improvements in and Analytical Applications of Advanced Ion Trap Technology. *Int. J. Mass Spectrom. Ion Process* **1984**, *60*, 85.
(27) Kaiser, R. E., Jr.; Louris, J. N.; Amy, J. W.; Cooks, R. G. Extending the Mass Range of the Quadrupole Ion Trap using Axial Modulation. *Rapid Commun. Mass Spectrom.* **1989**, *3* (7), 225−229.
(28) Richards, J. A.; Huey, R. M.; Hiller, J. A New Operating Mode for the Quadrupole Mass Filter. *Int. J. Mass Spectrom. Ion Phys.* **1973**, *12*, 317.
(29) Sheretov, E. P.; Terentiev, V. I. Theory of the Pulsed Quadrupole Mass Spectrometer. *Sov. Phys. Technol. Phys.* **1972**, *17* (5), 755.
(30) Sheretov, E. P.; Gurov, V. S.; Safonov, M. P.; Philippov, I. W. Hyperboloid Mass Spectrometers for Space Exploration. *Int. J. Mass Spectrom.* **1999**, *189*, 9.
(31) Ding, L.; Sudakov, M.; Kumashiro, S. A Simulation Study of the Digital Ion Trap Mass Spectrometer. *Int. J. Mass Spectrom.* **2002**, *221*, 117−138.

(32) Ensberg, E. S.; Jefferts, K. B. The Visible Photodissociation Spectrum of Ionized Methane. *Astrophys. J.* **1975**, *195*, L89−L91.
(33) Lawson, G.; Bonner, R. F.; Mather, R. E.; Todd, J. F. J.; March, R. E. Quadrupole Ion Store (QUISTOR). Part 1. Ion Molecule Reactions in Methane. *Water and Ammonia. J. Chem. Soc., Faraday Trans. 1* **1976**, *72*, 545−557.
(34) Armitage, M. A.; Higgins, M. J.; Lewars, E. G.; March, R. E. Methylketene. Ion Chemistry and Proton Affinity. *J. Am. Chem. Soc.* **1980**, *102*, 5064−5068.
(35) Brodbelt-Lustig, J.S.; Cooks, R.G. Determination of Relative Gas-Phase Basicities by the Proton Transfer Equilibrium Technique and the Kinetic Method in a Quadrupole Ion-Trap. *Talanta* **1989**, *36*, 255−260.
(36) Cooks, R. G.; Wong, P. S. Kinetic Method of Making Thermochemical Determinations: Advances and Applications. *Acc. Chem. Res.* **1998**, *31*, 379−386.
(37) Einhorn, J.; Kenttämaa, H. I.; Cooks, R. G. Information on the Location of Carbon-Carbon Double Bonds in C6-C23 Linear Alkenes from Carbon Addition Reactions in a Quadrupole Ion Trap Equipped with a Pulsed Sample-Inlet System. *J. Am. Soc. Mass Spectrom.* **1991**, *2*, 305−313.
(38) Louris, J. N.; Cooks, R. G.; Syka, J.E. P.; Kelley, P. E.; Stafford, G. C., Jr; Todd, J. F. J. Instrumentation, Applications, and Energy Deposition in Quadrupole Ion-Trap Tandem Mass Spectrometry. *Anal. Chem.* **1987**, *59*, 1677−1685.
(39) Hughes, R. J.; March, R. E.; Young, A. B. Multiphoton Dissociation of Ions Derived from 2-propanol in a QUISTOR with Low-Power CW Infrared Laser Radiation. *Int. J. Mass Spectrom Ion Phys.* **1982**, *42*, 255−263.
(40) Lammert, S. A.; Cooks, R. G. Surface-Induced Dissociation of Molecular ions in a Quadrupole Ion Trap Mass Spectrometer. *J. Am. Soc. Mass Spectrom.* **1991**, *2*, 487−491.
(41) Payne, A. H.; Glish, G. L. Thermally Assisted Infrared Multiphoton Photodissociation in a Quadrupole Ion Trap. *Anal. Chem.* **2001**, *73*, 3542−3548.
(42) Hashimoto, Y.; Hasegawa, H.; Yoshinari, K.; Waki, I. Collision-Activated Infrared Multiphoton Dissociation in a Quadrupole Ion Trap Mass Spectrometer. *Anal. Chem.* **2003**, *75*, 420−425.
(43) Boué, S. M.; Stephenson, J. L., Jr; Yost, R. A. Pulsed Helium Introduction into a Quadrupole Ion Trap for Reduced Collisional Quenching during Infrared Multiphoton Dissociation of Electrosprayed Ions. *Rapid Commun. Mass Spectrom.* **2000**, *14*, 1391−1397.
(44) Gabryelski, W.; Li, L. Photo-Induced Dissociation of Electrospray Generated Ions in an Ion Trap/Time-of-Flight Mass Spectrometer. *Rev. Sci. Instrum.* **1999**, *70*, 4192−4199.
(45) Wilson, J. J.; Brodbelt, J. S. MS/MS Simplification by 355nm Ultraviolet Photodissociation of Chromophore-Derivatized Peptides in a Quadrupole Ion Trap. *Anal. Chem.* **2007**, *79*, 7883−7892.
(46) Stephenson, J. L., Jr.; McLuckey, S. A. Ion/Ion Proton Transfer Reactions for Protein Mixture Analysis. *Anal. Chem.* **1996**, *68*, 4026−4032.
(47) Chrisman, P. A.; Pitteri, S. J.; McLuckey, S. A. Parallel Ion Parking of Protein Mixtures. *Anal. Chem.* **2006**, *78*, 310−316.
(48) Herron, W. J.; Goeringer, D. E.; McLuckey, S. A. Gas-Phase Electron Transfer Reactions from Multiply-Charged Anions to Rare Gas Cations. *J. Am. Chem. Soc.* **1995**, *117*, 11555−11562.
(49) Huzarska, M.; Ugalde, I.; Kaplan, D. A.; Hartmer, R.; Easterling, M. L.; Polfer, N. C. Negative Electron Transfer Dissociation of Deprotonated Phosphopeptide Anions: Choice of Radical Cation Reagent and Competition between Electron and Proton Transfer. *Anal. Chem.* **2010**, *82*, 2873−2878.
(50) He, M.; McLuckey, S. A. Two Ion/Ion Charge Inversion Steps to form a Doubly Protonated Peptide from a Singly Protonated Peptide in the Gas Phase. *J. Am. Chem. Soc.* **2003**, *125*, 7756−7757.
(51) Kjeldsen, F.; Silivra, O. A.; Ivonin, I. A.; Haselmann, K. F.; Gorshkov, M.; Zubarev, R. A. Cα-C Backbone Fragmentation Dominates in Electron Detachment Dissociation of Gas-Phase Polypeptide Polyanions. *Chem.—Eur. J.* **2005**, *11*, 1803−1812.
(52) Misharin, A. S.; Silivra, O. A.; Kjeldsen, F.; Zubarev, R. A. Dissociation of Peptide Ions by Fast Atom Bombardment in a Quadrupole Ion Trap. *Rapid Commun. Mass Spectrom.* **2005**, *19*, 2163−2171.
(53) Cook, S. L.; Collin, O. L.; Jackson, G. P. Metastable Atom-Activated Dissociation Mass Spectrometry: Leucine/Isoleucine Differentiation and Ring Cleavage of Proline Residues. *J. Mass Spectrom.* **2009**, *44*, 1211−1223.
(54) Cook, S. L.; Jackson, G. P. Metastable Atom-Activated Dissociation Mass Spectrometry of Phosphorylated and Sulfonated Peptides in Negative Ion Mode. *J. Am. Soc. Mass Spectrom.* **2011**, *22*, 1088−1099.
(55) Takahashi, H.; Sekiya, S.; Nishikaze, T.; Kodera, K.; Iwamoto, S.; Wada, M.; Tanaka, K. Hydrogen Attachment/Abstraction Dissociation (HAD) of Gas Phase Peptide Ions for Tandem Mass Spectrometry. *Anal. Chem.* **2016**, *88*, 3810−3816.
(56) Takahashi, H.; Shimabukuro, Y.; Asakawa, D.; Yamauchi, S.; Sekiya, S.; Iwamoto, S.; Wada, M.; Tanaka, K. Structural Analysis of Phospholipid using Hydrogen Abstraction Dissociation and Oxygen Attachment Dissociation in Tandem Mass Spectrometry. *Anal. Chem.* **2018**, *90*, 7230−7238.
(57) Soni, M. H.; Cooks, G. R. Selective Injection and Isolation of Ions in Quadrupole Ion Trap Mass Spectrometry using Notched Waveforms Created using Inverse Fourier Transform. *Anal. Chem.* **1994**, *66*, 2488−2496.
(58) Schwartz, J. C.; Senko, M. W.; Syka, J. E. P. A Two-Dimensional Quadrupole Ion Trap Mass Spectrometer. *J. Am. Soc. Mass Spectrom.* **2002**, *13*, 659−669.
(59) Hager, J. W. A New Linear Ion Trap Mass Spectrometer. *Rapid Commun. Mass Spectrom.* **2002**, *16*, 512−526.
(60) Pekar-Second, T. P.; Blethrow, J. D.; Schwartz, J. C.; Merrihew, G. E.; MacCoss, M. J.; Swaney, D. L.; Russell, J. D.; Coon, J. J.; Zabrouskov, V. Dual-Pressure Linear Ion Trap Mass Spectrometer Improving the Analysis of Complex Protein Mixtures. *Anal. Chem.* **2009**, *81*, 7757−7765.
(61) Olsen, J. V.; Schwartz, J. C.; Griep-Raming, J.; Nielsen, M. L.; Damoc, E.; Denisov, E.; Lange, O.; Remes, P.; Taylor, D.; Splendore, M.; Wouters, E. R.; Senko, M.; Makarov, M.; Mann, M.; Horning, S. A Dual Pressure Linear Ion Trap Instrument with Very High Sequencing Speed. *Mol. Cell. Proteom.* **2009**, *8*, 2759−2769.
(62) Kim, T. Y.; Thompson, M. S.; Reilly, J. P. Peptide Photodissociation at 157 nm in a Linear Ion Trap Mass Spectrometer. *Rapid Commun. Mass Spectrom.* **2005**, *19*, 1657−1665.
(63) Fung, E. Y. M.; Kjeldsen, F.; Silivra, O. A.; Chan, D. T. W.; Zubarev, R. A. Facile Disulfide Bond Cleavage in Gaseous Peptide and Protein Cations by Ultraviolet Photodissociation at 157 nm. *Angew. Chem., Int. Ed.* **2005**, *44*, 6399−6403.
(64) Kjeldsen, F.; Silivra, O. A.; Zubarev, R. A. Zwitterionic States in Gas-Phase Polypeptide Ions Revealed by 157-nm Ultra-Violet Photodissociation. *Chem.—Eur. J.* **2006**, *12*, 7920−7928.
(65) Syka, J. E. P.; Coon, J. J.; Schroeder, M. J.; Shabanowitz, J.; Hunt, D. F. Peptide and Protein Sequence Analysis by Electron Transfer Dissociation Mass Spectrometry. *Proc. Natl. Acad. Sci. U.S.A.* **2004**, *101*, 9528−9533.
(66) Riley, N. M.; Westphall, M. S.; Hebert, A. S.; Coon, J. J. Implementation of Activated Ion Electron Trabsfer Disosciation in a Quadrupole-Orbitrap-Linear Ion Trap Hybrid Mass Spectrometer. *Anal. Chem.* **2017**, *89*, 6358−6366.
(67) Frese, C. K.; Altelaar, A. F. M.; van den Toorn, H.; Nolting, D.; Griep-Raming, J.; Heck, A. J. R.; Mohammed, S. Toward Full Peptide Sequence Coverage by Dual Fragmentation Combining Electron-Transfer and Higher-Energy Collision Dissociation Tandem Mass Spectrometry. *Anal. Chem.* **2012**, *84*, 9668−9673.
(68) Ugrin, S. A.; English, A. M.; Syka, J. E. P.; Bai, D. L.; Anderson, L. C.; Shabanowitz, J.; Hunt, D. F. Ion-Ion Proton Transfer and Parallel Ion Parking for the Analysis of Mixtures of Intact Proteins on a Modified Orbitrap Mass Analyzer. *J. Am. Soc. Mass Spectrom.* **2019**, *30*, 2163−2173.

https://doi.org/10.1021/jasms.2c00214
J. Am. Soc. Mass Spectrom. 2022, 33, 1990−2007

(69) Klein, D. R.; Holden, D. D.; Brodbelt, J. S. Shotgun Analysis of Rough-Type Lipopolysaccharides using Ultraviolet Photodissociation Mass Spectrometry. *Anal. Chem.* **2016**, *88*, 1044−1051.
(70) Lai, C. K.; Ng, D. C. M.; Pang, H. F.; Yves Le Blanc, J. C.; Hager, J. W.; Fang, D. C.; Cheung, A. S. C.; Chu, I. K. Laser-Induced Photodissociation of Singly Protonated Peptides at 193 and 266nm within a Hybrid Linear Ion Trap Mass Spectrometer. *Rapid Commun. Mass Spectrom.* **2013**, *27*, 1119−1127.
(71) Shaw, J. B.; Li, W.; Holden, D. D.; Zhang, Y.; Griep-Raming, J.; Fellers, R. T.; Early, B. P.; Thomas, P. M.; Kelleher, N. L.; Brodbelt, J. S. Complete Protein Characterization Using Top-Down Mass Spectrometry and Ultraviolet Photodissociation. *J. Am. Chem. Soc.* **2013**, *135* (34), 12646−12651.
(72) Halim, M. A.; Girod, M.; MacAleese, L.; Lemoine, J.; Antoine, R.; Dugourd, P. Combined Infrared Multiphoton Dissociation with Ultraviolet Photodissociation for Ubiquitin Characterization. *J. Am. Soc. Mass Spectrom.* **2016**, *27*, 1435−1442.
(73) Satake, H.; Hasegawa, H.; Hirabayashi, A.; Hashimoto, Y.; Baba, T. Fast Multiple Electron Capture Dissociation in a Linear Radio Frequency Quadrupole Ion Trap. *Anal. Chem.* **2007**, *79*, 8755−8761.
(74) Baba, T.; Ryumin, P.; Duchoslav, E.; Chen, K.; Chelur, A.; Loyd, B.; Chernushevich, I. Dissociation of Biomolecules by an Intense Low-Energy Electron Beam in a High Sensitivity Time-of-Flight Mass Spectrometer. *J. Am. Soc. Mass Spectrom.* **2021**, *32*, 1964−1975.
(75) Lössl, P.; van der Waterbeemd, M.; Heck, A. J. R. The Diverse and Expanding Role of Mass Spectrometry in Structural and Molecular Biology. *EMBO J.* **2016**, *35*, 2634−2657.
(76) Ly, T.; Julian, R. R. Residue-Specific Radical-Directed Dissociation of whole Proteins in the Gas Phase. *J. Am. Chem. Soc.* **2008**, *130*, 351−358.
(77) Hoffmann, W. D.; Jackson, G. P. Charge Transfer Dissociation (CTD) Mass Spectrometry of Peptide Cations using Kiloelectronvolt Helium Cations. *J. Am. Soc. Mass Spectrom.* **2014**, *25*, 1939−1943.
(78) Chingin, K.; Makarov, A.; Denisov, E.; Rebrov, O.; Zubarev, R. R. Fragmentation of Positively-Charged Biological Ions Activated with a Beam of High-Energy Cations. *Anal. Chem.* **2014**, *86*, 372−379.
(79) Milosavljevic, A. R.; Nicolas, C.; Lemaire, J.; Dehon, C.; Thissen, R.; Bizau, J. M.; Refregiers, M.; Nahona, L.; Guiliani, A. Photoionization of a protein isolated in vacuo. *Phys. Chem. Chem. Phys.* **2011**, *13*, 15432−15436.
(80) Berkout, V. D.; Doroshenko, V. D. Fragmentation of Phosphorylated and Singly Charged Peptide Ions via Interaction with Metastable Atoms. *Int. J. Mass Spectrom.* **2008**, *278*, 150−157.
(81) Rizzo, R. T.; Boyarkin, O. V. Cryogenic Methods for the Spectroscopy of Large, Biomolecular Ions. *Top. Curr. Chem.* **2014**, *364*, 43−98.
(82) Brabeck, G. F.; Chen, H.; Hoffman, N. M.; Wang, L.; Reilly, P. T. A. Development of MS(n) in Digitally Operated Linear Ion Guides. *Anal. Chem.* **2014**, *86*, 7757−7763.
(83) Ding, L.; Brancia, F. L. Electron Capture Dissociation in a Digital Ion Trap Mass Spectrometer. *Anal. Chem.* **2006**, *78*, 1995−2000.
(84) Kasper, T.; Hoener, M.; Papanastasiou, D.; Lekkas, A.; Kounadis, D.; Orfanopoulos, I. A Novel Instrument Platform for the Investigation of Particle Formation from the Gas Phase. *67th Conference on Mass Spectrometry and Allied Topics*, WP466, Atlanta, GA, June 2−6, 2019.
(85) Ding, L.; Sudakov, M.; Brancia, F. L.; Giles, R.; Kumashiro, S. A Digital Ion Trap Mass Spectrometer Coupled with Atmospheric Pressure Ion Sources. *J. Mass Spectrom.* **2004**, *39*, 471−484.
(86) Kosmopoulou, M.; Smyrnakis, A.; Papanastasiou, D.; Fort, K.; Makarov, A.; Zubarev, R. A.: Top Down Analysis of Intact Antibodies under Denatured and Native Conditions on the Omnitrap Platform coupled to an Orbitrap Mass Analyzer. *68th Conference on Mass Spectrometry and Allied Topics - Reboot*, ThP548, June 1−12, 2020.
(87) *SIMION 8.0 Scientific Instrument Services Inc.*; Scientific Instrument Services, Inc., 2012.
(88) Di Stefano, L.; Papanastasiou, D.; Zubarev, R. A. Size-Dependent Hydrogen Atom Attachment to Gas-Phase Hydrogen-Deficient Polypeptide Radical Cations. *J. Am. Chem. Soc.* **2018**, *140*, 531−533.
(89) Konenkov, N. V.; Sudakov, M.; Douglas, D. J. Matrix Methods for the Calculation of Stability Diagrams in Quadrupole Mass Spectrometry. *J. Am. Soc. Mass Spectrom.* **2002**, *13* (6), 597−613.
(90) Koizumi, H.; Whitten, W. B.; Reilly, P. T. A. Derivation of Mathematical Expressions to Define Resonant Ejection from Square and Sinusoidal Wave Ion Traps. *Int. J. Mass Spectrom.* **2009**, *286*, 64−69.
(91) Li, J.; Taraszka, J. A.; Counterman, A. E.; Clemmer, D. E. Influence of solvent Composition and Capillary Temperature on the Conformations of Electrosprayed Ions: Unfolding of Compact Ubiquitin Conformers from Pseudonative and Denatured Solutions. *Int. J. Mass Spectrom.* **1999**, *185−187*, 37−47.
(92) Reid, G. E.; Wu, J. H.; Chrisman, P. A.; Wells, J. M.; McLuckey, S. A. Charge-State-Dependent Sequence Analysis of Protonated Ubiquitin Ions via Ion Trap Tandem Mass Spectrometry. *Anal. Chem.* **2001**, *73*, 3274−3281.
(93) Zubarev, R. A.; Horn, D. M.; Fridriksson, E. K.; Kelleher, N. L.; Kruger, N. A.; Lewis, M. A.; Carpenter, B. K.; McLafferty, F. W. Electron Capture Dissociation for Structural Characterization of Multiply Charged Proteins Cations. *Anal. Chem.* **2000**, *72*, 563−573.
(94) Breuker, K.; Oh, H.; Horn, D. M.; Cerda, B. A.; McLafferty, F. W. Detailed Unfolding and Folding of Gaseous Ubiquitin Ions Characterized by Electron Capture Dissociation. *J. Am. Chem. Soc.* **2002**, *124*, 6407−6420.
(95) Cooper, H. J. Investigation of the Presence of b Ions in Electron Capture Dissociation Mass Spectra. *J. Am. Soc. Mass Spectrom.* **2005**, *16* (12), 1932−1940.
(96) Zubarev, R. A.; Good, D. M.; Savitski, M. M. Radical a-ions in Electron Capture Dissociation: On the Origin of Species. *J. Am. Soc. Mass Spectrom.* **2012**, *23*, 1015−1018.
(97) Fort, K.; Cramer, C. N.; Voinov, V. G.; Vasil'ev, Y. V.; Lopez, N. I.; Beckman, J. S.; Heck, A. J. R. Exploring ECD on a Benchtop Q Exactive Orbitrap Mass Spectrometer. *J. Proteome Res.* **2018**, *17* (2), 926−933.
(98) Robinson, E. W.; Leib, R. D.; Williams, E. R. The Role of Conformation on Electron Capture Dissociation of Ubiquitin. *J. Am. Soc. Mass Spectrom.* **2006**, *17*, 1470−1479.
(99) Fung, E. Y. M.; Adams, C. M.; Zubarev, R. A. Electron Ionization Dissociation of Singly and Multiply Charged Peptides. *J. Am. Chem. Soc.* **2009**, *131*, 9977−9985.
(100) Chen, X.; Wang, Z.; Wong, Y.-L. E.; Wu, R.; Zhang, F.; Chan, T-W.D. Electron-ion reaction-based dissociation: A powerful ion activation method for the elucidation of natural product structures. *Mass Spectrom. Reviews.* **2018**, *37*, 793.
(101) Sasiene, Z. J.; Mendis, P. M.; Jackson, G. P. Quantitative Assessment of Six Different Reagent Gases for Charge Transfer Dissociation (CTD) of Biological Ions. *Int. J. Mass Spectrom.* **2021**, *462*, 116532.
(102) Bari, S.; Hoekstra, R.; Schlatholter, T. Peptide Fragmentation by keV ion-induced Dissociation. *Phys. Chem. Chem. Phys.* **2010**, *12*, 3376−3383.
(103) Ickert, S.; Beck, S.; Linscheid, M. W.; Riedel, J. VUV Photodissociation Induced by a Deuterium Lamp in an Ion Trap. *J. Am. Soc. Mass Spectrom.* **2019**, *30*, 2114−2122.
(104) Papanastasiou, D.; Lekkas, A.; Kounadis, D.; Orfanopoulos, I.; Mpozatzidis, A.; Raptakis, E. Ion-ion and Ion-Electron Activation Experiments in a Novel Linear Ion Trap. *63rd Conference on Mass Spectrometry and Allied Topics*, TP03-046, St. Louis, MO, May 31−June 4, 2015.
(105) Raptakis, E.; Papanastasiou, D.; Klaeger, S.; Clauser, K.; Keshishian, H.; Carr, S. A. Electron Induced Dissociation of class I HLA peptides Provides Increased Sequence Coverage Compared to Collision-induced Dissociation. *66th Conference on Mass Spectrometry and Allied Topics*, ThP-578, San Diego, CA, June 3−7, 2018.

https://doi.org/10.1021/jasms.2c00214
J. Am. Soc. Mass Spectrom. 2022, 33, 1990−2007

(106) Nielsen, M. L.; Budnik, B. A.; Haselmann, K. F.; Olsen, J. V.; Zubarev, R. A. Intramolecular Hydrogen Atom Transfer in Hydrogen-Deficient Polypeptide Radical Cations. *Chem. Phys. Lett.* **2000**, *330*, 558−562.
(107) Kosmopoulou, M.; Papanastasiou; Zubarev, R. A. Multiple-Stage Tandem Mass Spectrometry of Peptide Radical Ions in the Omnitrap Platform. *67th Conference on Mass Spectrometry and Allied Topics*, MP-239, Atlanta, GA, June 2−6, 2018.
(108) Li, H.; Sheng, Y.; McGee, W.; Cammarata, M.; Holden, D.; Loo, J. A. Structural Characterization of Native Proteins and Protein Complexes by Electron Ionization Dissociation-Mass Spectrometry. *Anal. Chem.* **2017**, *89*, 2731−2738.
(109) Shaw, J. B.; Li, W.; Holden, D. D.; Zhang, Y.; Griep-Raming, J.; Fellers, R. T.; Early, B. P.; Thomas, P. M.; Kelleher, N. L.; Brodbelt, J. S. Complete protein characterization using top-down mass spectrometry and ultraviolet photodissociation. *J. Am. Chem. Soc.* **2013**, *135* (34), 12646−12651.
(110) Riley, N. M.; Westphall, M. S.; Coon, J. J. Activated Ion-Electron Transfer Dissociation Enables Comprehensive Top-Down Protein Fragmentation. *J. Proteome Res.*, **2017**, *16* (7), 2653−2659.

https://doi.org/10.1021/jasms.2c00214
J. Am. Soc. Mass Spectrom. 2022, 33, 1990−2007